Am J Physiol Heart Circ Physiol 297: H1776–H1782, 2009.
First published September 4, 2009; doi:10.1152/ajpheart.00050.2009.

Adenylyl cyclase type 5 protein expression during cardiac development and stress

Che-Lin Hu,* Rachna Chandra,* Hui Ge, Jayashree Pain, Lin Yan, Gopal Babu, Christophe Depre, Kousaku Iwatsubo, Yoshihiro Ishikawa, Junichi Sadoshima, Stephen F. Vatner, and Dorothy E. Vatner

Department of Cell Biology and Molecular Medicine and the Cardiovascular Research Institute at the University of Medicine and Dentistry of New Jersey, New Jersey Medical School, Newark, New Jersey

Submitted 14 January 2009; accepted in final form 29 July 2009

Hu C, Chandra R, Ge H, Pain J, Yan L, Babu G, Depre C, Iwatsubo K, Ishikawa Y, Sadoshima J, Vatner SF, Vatner DE. Adenylyl cyclase type 5 protein expression during cardiac development and stress. *Am J Physiol Heart Circ Physiol* 297: H1776–H1782, 2009. First published September 4, 2009; doi:10.1152/ajpheart.00050.2009.— Adenylyl cyclase (AC) types 5 and 6 (AC5 and AC6) are the two major AC isoforms expressed in the mammalian heart that mediate signals from β-adrenergic receptor stimulation. Because of the unavailability of isoform-specific antibodies, it is difficult to ascertain the expression levels of AC5 protein in the heart. Here we demonstrated the successful generation of an AC5 isoform-specific mouse monoclonal antibody and studied the expression of AC5 protein during cardiac development in different mammalian species. The specificity of the antibody was confirmed using heart and brain tissues from AC5 knockout mice and from transgenic mice overexpressing AC5. In mice, the AC5 protein was highest in the brain but was also detectable in all organs studied, including the heart, brain, lung, liver, stomach, kidney, skeletal muscle, and vascular tissues. Western blot analysis showed that AC5 was most abundant in the neonatal heart and declined to basal levels in the adult heart. AC5 protein increased in the heart with pressure-overload left ventricular hypertrophy. Thus this new AC5 antibody demonstrated that this AC isoform behaves similarly to fetal type genes, such as atrial natriuretic peptide; i.e., it declines with development and increases with pressure-overload hypertrophy.

adenylyl cyclase isoforms; monoclonal antibody; pressure overload; hypertrophy

ADENYLYL CYCLASE (AC) is an enzyme that catalyzes the conversion of ATP to cAMP. The complexity in understanding the signaling pathway of cAMP can be attributed, in part, to 10 isoforms of AC: nine membrane bound and one soluble, which have been cloned and characterized in mammals (4, 6, 9, 10, 29). Each of these membrane-bound isoforms consists of two hydrophobic domains (with 6 transmembrane spans) and two cytoplasmic domains. The cytoplasmic domains constitute the catalytic site, which is subject to intracellular regulation (6). The AC isoforms have high amino acid homology in their cytoplasmic domains but differ in the sequence of the transmembrane region. The specificity of tissue distribution, the functional properties, and the chromosomal location of the corresponding genes also differentiate these isoforms (4, 10, 12). The major AC isoforms expressed in the heart are type 5 (AC5) and type 6 (AC6) (7, 11, 30). Tissue distribution and developmental expression of AC5 and AC6 mRNA have been previously studied in rats, chicks, and humans (7, 30, 31). However, in the absence of an AC5-specific antibody, it has not been possible to determine the levels of protein expression. It is very important to study the differential regulation of AC5 and AC6 in the heart since AC5 and AC6 behave differently in the pathogenesis of heart failure. We demonstrated that the AC5 knockout (KO) mouse model lives longer and is resistant to stress (32), including chronic pressure overload (21) and chronic catecholamine (22) stress. However, studies by others have suggested that the overexpression of AC6 is beneficial and might be considered for heart failure therapy (23). In addition, based on mRNA measurements, conflicting data have been presented regarding the ontogeny of AC5 (7, 26, 30). All of the important studies related to AC5 in the heart are limited by the absence of a specific antibody. Accordingly, the first goal of this investigation was to develop an AC5-specific monoclonal antibody and then to determine the expression levels of AC5 protein during a physiological process and cardiac development and in response to pathophysiological stress induced by chronic pressure overload.

MATERIALS AND METHODS

Antibody preparation and purification. The peptide sequence NH_2-GNQVSKEMKRMGFEDPKDKN-COOH, which is specific to the cytoplasmic domain (C1b portion) of the AC5 protein and has the least homology with the other AC isoforms, was used to generate the mouse monoclonal antibody. The synthetic peptide (Rockland Immunochemicals, Gilbertville, PA) was conjugated to keyhole limpet hemocyanin to impart immunogenicity to the small peptide and then mixed with adjuvant (Titermax Gold for the first injection and Freund's incomplete adjuvant for subsequent booster doses) and used to immunize Balb/C mice. The fusion of mouse spleen with mouse myeloma cells, Sp2/0, was done using standard hybridoma techniques (17). The selection of the antibody was done by screening the supernatant by ELISA and using the synthetic peptide as an antigen. The CELLine device CL-1000 (BD Biosciences) was used for producing the monoclonal antibody in high yield. Cells were harvested by centrifugation at 3,500 *g* for 1 h at 4°C. The monoclonal antibody in the supernatant fraction was precipitated with ice-cold ammonium sulfate solution (pH 7.4). The antibody pellet was dissolved in PBS and dialyzed against the same buffer. The dialysate was centrifuged at 10,000 *g* for 30 min at 4°C to remove aggregates, if any. The supernatant fraction was filtered through a 0.2-mm filter and further purified by immunoaffinity chromatography using a protein G column (Pierce Biotechnology) following the manufacturer's protocol.

Animal models. The transgenic (TG) mouse with cardiac overexpression of AC5 was generated by the insertion of the coding region of the canine AC5 gene (4.3 kb, gene bank accession no. M88649; cloned by Dr. Ishikawa) to a vector containing the mouse α-myosin heavy chain gene promoter region (gene bank accession no. U71441)

* C.-L. Hu and R. Chandra contributed equally to this work.

Address for reprint requests and other correspondence: D. E. Vatner, Univ. of Medicine & Dentistry of New Jersey-New Jersey Medical School, Dept. of Cell Biology & Molecular Medicine, 185 S. Orange Ave., MSB G609, Newark, NJ 07103 (e-mail: vatnerdo@umdnj.edu).

in a pBlueScript vector followed by poly(A) sequence of the human growth hormone gene. The AC6 TG construct was done similarly by inserting the coding region of the canine AC6 gene (4 kb, gene bank accession no. M94968; cloned by Dr. Ishikawa) into the same vector. AC5 KO (20) and wild-type (WT) mice and 129SVJ mice were also

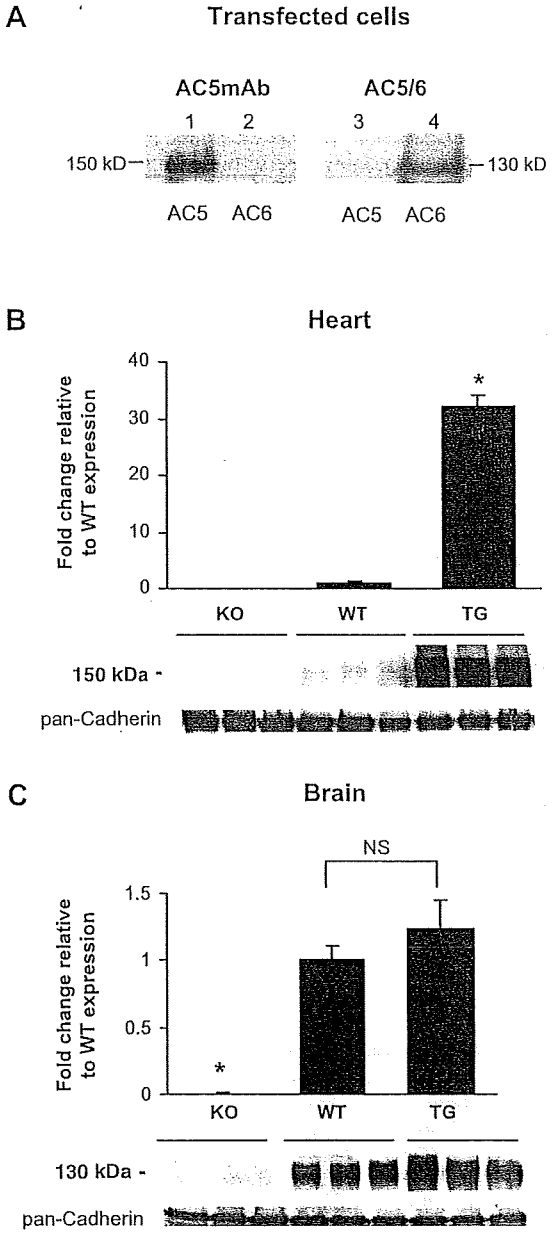

Fig. 1. Specificity of the adenylyl cyclase type 5 (AC5) mouse monoclonal antibody (AC5MAb). *A*: equal amounts of lysates from COS-7 cells transfected with AC5 cDNA (*lane 1*) and AC6 cDNA (*lane 2*) were immunoblotted with AC5MAb. The lysates from COS-7 cells transfected with AC5 cDNA (*lane 3*) and AC6 cDNA (*lane 4*) were immunoblotted with AC5/6 commercial antibody from Santa Cruz. Membrane preparations from the whole heart (*B*) and brain (*C*) of AC5 knockout (KO), wild-type (WT), and cardiac-specific AC5 transgenic (TG) mouse models (n = 7 to 8) were resolved on a 6% SDS-PAGE and immunoprobed with AC5MAb. The data are normalized to the value of WT samples and expressed as means ± SE. The loading control is shown using pan-cadherin antibody. *$P < 0.05$ vs. all other groups. NS, not significantly different.

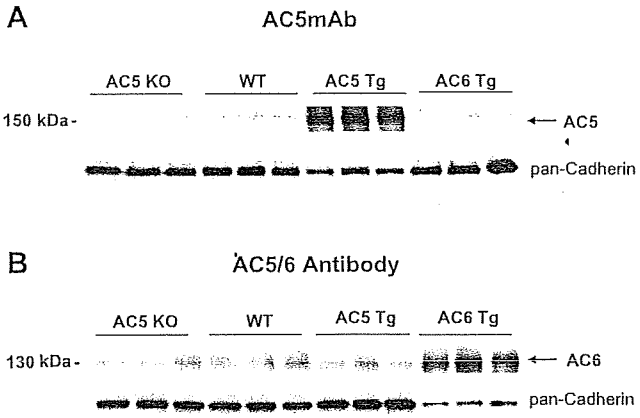

Fig. 2. Western blot analysis of AC5MAb with mouse heart. *A*: AC5 protein is detected by immunoblotting and is absent in AC5 KO and increased in AC5 TG hearts. The level of AC5 was similar to WT in the AC6 TG mouse heart. The amount of protein loaded from AC5 TG heart is 50% of the amount from AC5 KO, WT, and AC6 TG hearts. *B*: immunoblot using an AC5/6 commercial antibody. The AC levels were not different in hearts of AC5 KO, WT, and AC5 TG but increased in AC6 TG hearts, indicating that this antibody may primarily detect only AC6 protein. The amount of protein loaded from AC6 TG heart is 30% of the amount from AC5 KO, WT, and AC5 TG hearts. The loading control is shown using pan-cadherin antibody.

used for ontogenic studies. Commercially available Sprague-Dawley rats and mixed-breed pigs (n = 4 per age group) were used for ontogenic studies. FVB mice were used for transverse aortic banding (25) to induce left ventricular hypertrophy (LVH). At 4 to 5 mo of age, the mice were anesthetized with a mixture of ketamine (65 mg/kg), xylazine (2 mg/kg), and acepromazine (13 mg/kg). A thoracotomy was performed and the transverse aorta was constricted by placing a suture around a 28-gauge needle. The needle was removed and the chest closed. A similar procedure was performed on sham-operated mice without the placement of the suture. After 4 wk of

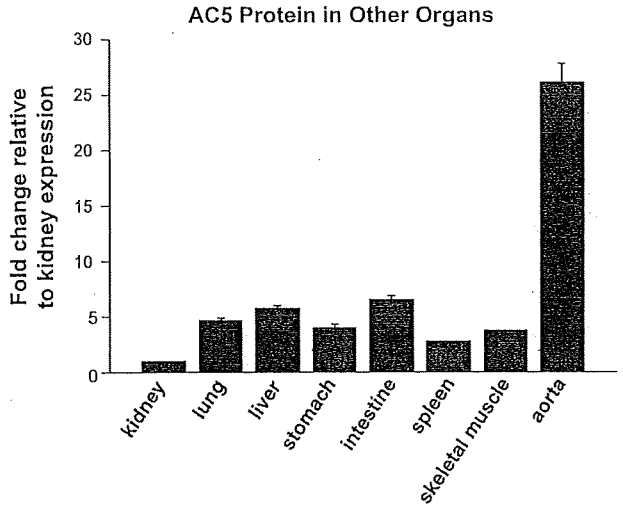

Fig. 3. Tissue distribution of AC5 protein expression in young pigs (2 to 3 mo, n = 4). With the use of Western blot analysis, the level of AC5 protein expression was measured in kidney, lung, liver, stomach, intestine, spleen, skeletal muscle, and vascular tissues. The number of samples exceeded that which could be run on one gel, and, accordingly, samples were run on 3 distinct gels; each gel contained the same kidney sample as a control. All data were quantitated with densitometry and normalized to the value of kidney samples. Data are expressed as means ± SE.

aortic banding, the mouse hearts were harvested and studied. These studies were approved by the Institutional Animal Care and Use Committee of the New Jersey Medical School.

AC5 and AC6 transfection. COS-7 cells were infected with 2 μg of AC5 or AC6 cDNA plasmid, respectively, using 6 μl of Fugene 6 transfection reagent (Roche Applied Science). After 48 h, the cells were harvested, washed twice with PBS, and lysed for 30 min with lysis buffer consisting of 50 mM Tris·HCl, 50 mM NaCl, and 1% Tergitol-type nonyl phenoxylpolyethoxylethanol-40 (NP-40) with protease inhibitors. After centrifugation at 4°C, the lysate was stored in aliquots at −80°C and 15 μg of protein were used for Western blot analysis.

Western blot analysis. The frozen heart and brain tissues from mice, rats, and pigs were homogenized on ice in buffer containing (in mM) 50 Tris·HCl, 6 $MgCl_2$, 75 sucrose, 1 dithiothreitol, and 1 EDTA (pH 7.6) (TMSDE buffer) and 1 phenylmethylsulphonyl fluoride. The homogenate was centrifuged at 600 *g* for 8 min at 4°C, and the supernatant was centrifuged again at 69,000 *g* for 60 min at 4°C to collect the membrane proteins. The membrane pellet was resuspended in TMSDE buffer containing 1% NP-40 and briefly sonicated. The protein concentration was determined with the bicinchoninic acid method (Pierce Biotechnology, Rockford, IL). The membrane sample was solubilized in loading buffer, containing 62.5 mM Tris·HCl (pH 6.8), 25% glycerol, 2% SDS, and 0.1% bromophenol blue, and was separated on a 6% SDS polyacrylamide gel, as previously described (16). The proteins were then transferred to a nitrocellulose membrane and blocked for 1 h with 5% milk in buffer containing 20 mM Tris·HCl (pH 7.5), 150 mM NaCl, and 0.1% Tween-20 (TBST). The membranes were incubated with our affinity-purified, AC5 mouse monoclonal antibody (AC5MAb, 1:500 dilution) or the commercial AC5/6 antibody (C-17) (1:200 dilution; Cat. No. sc-590; Santa Cruz Biotechnology, Santa Cruz, CA) at 4°C overnight. After incubation with the primary antibody, the blots were then washed with TBST at room temperature and incubated with goat anti-mouse IgG [heavy and light chains (H+L)] (for AC5 detection) or goat anti-rabbit IgG (H+L) (for AC6 detection)-horseradish peroxidase-conjugated secondary antibody for 30 min. Immunoreactive bands were detected with Western Lightning Chemiluminescence Reagent (Perkin Elmer Life Sciences, Boston, MA). All Western blot exposures were in the linear range of detection, and the intensities of the resulting bands were quantified by Quantity One software on GS-800 densitometer (Bio-Rad, Hercules, CA). The plasma membrane marker, pan-cadherin antibody, was used as a loading control.

Northern blot analysis. Total RNA was isolated from heart tissue that was previously dissected and frozen in liquid nitrogen using the TriReagent isolation method according to the manufacturer's instructions (Sigma, St. Louis, MO). A total of 20 μg of total RNA was separated on a 1.2% agarose gel containing 1× 3-[*N*-morpholino]propanesulfonic acid and 2% formaldehyde. RNA was then transferred onto a nylon membrane. The membranes were hybridized overnight in PerfectHyb solution (Sigma) containing α-P^{32}-dCTP-labeled AC5-specific probe (a fragment corresponding to nucleotides 1929 to 2129 relative to the initiation of methionine codon). The membranes were washed with 2× saline-sodium citrate (0.3 M sodium chloride and 30 mM sodium citrate), 0.1% SDS buffer

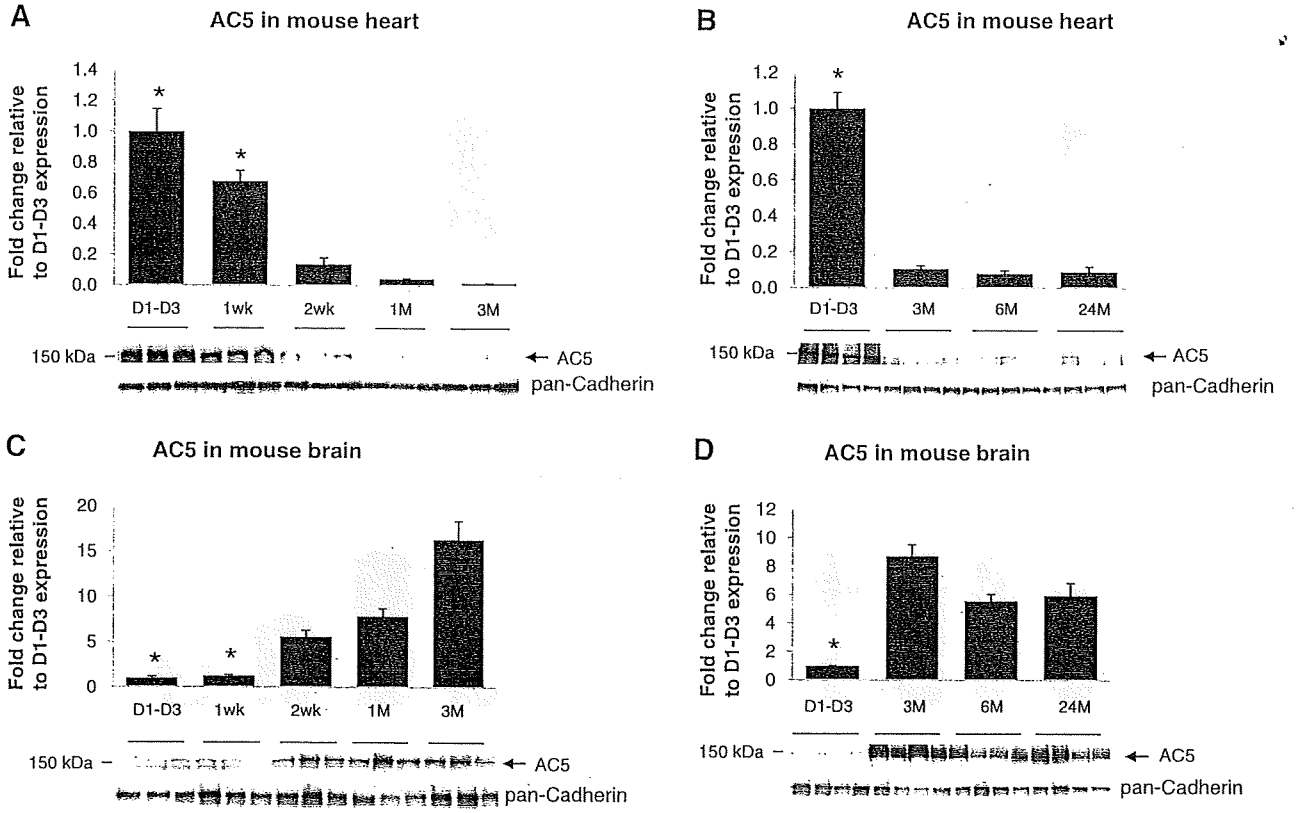

Fig. 4. AC5 protein levels in WT mouse heart and brain tissues. Immunoblotting was performed with AC5MAb using mouse heart and brain homogenates. Western blots were run individually for each age group: *neonatal day 1–day 3* (*D1–D3*), 1 wk, 2 wk, 1 mo (1M), and 3 mo (3M), from mouse heart (n = 3/age group) (*A*); *D1–D3*, 3 mo, 6 mo (6M), and 24 mo (24M) from mouse heart (n = 4/age group) (*B*); and *D1–D3*, 1 wk, 2 wk, 1 mo, and 3 mo from mouse brain (n = 3/age group) (*C*); and *D1–D3*, 3 mo, 6 mo, and 24 mo from mouse brain (n = 4/age group) (*D*). AC5 protein was highest in mouse neonatal heart and lowest in mouse neonatal brain (before 1 wk) compared with adult (*$P < 0.05$ vs. other groups). Data are normalized to mouse *D1–D3* samples and expressed as means ± SE.

for 2× 5 min and 0.1× saline-sodium citrate, and 0.1% SDS buffer for 2× 10 min before exposure for autoradiography.

Quantitative real-time polymerase chain reaction. The expression of AC5 mRNA levels was quantified using real-time PCR (ABI Prism 7300). From each sample, 50 ng of total RNA were reverse transcribed (TaqMan, Applied Biosystems) at 42°C for 30 min. The absolute quantification of AC5 and AC6 transcript was measured by TaqMan Probe real-time PCR assays with mouse-specific AC5 forward primer: 5′-CACAATCCGCCTCACTGG-3′, reverse primer: 5′-TCCTCAAAGCCCATCCTCTT-3′, and AC5-specific probe: 5′-/56-FAM/AGCCGAGCGCCCCTTCTACAA/36-TAMTSp/-3′. Real-time PCR was performed in two steps: a 1-min step at 95°C, followed by 40 cycles of a 12-s step at 95°C and a 1-min step at 60°C. Internal standards were prepared for each transcript from their PCR-amplified cDNA (5). Data normalization was performed by quantitative PCR amplification of cyclophilin gene or 18S rRNA.

Statistical analysis. Statistical analysis was performed using StatView 5.0 statistical software (SAS Institute). The data are reported as means ± SE. Comparisons between two groups were conducted with Student's *t*-test. Multiple group comparisons were performed by ANOVA. Significance was recorded for $P < 0.05$.

RESULTS

Characterization of AC5-specific mouse monoclonal antibody. First, we determined the specificity of the AC5 monoclonal antibody (AC5MAb) by Western blot analysis using AC5 or AC6 recombinant proteins expressed in COS-7 cells. As seen in Fig. 1*A* (*lane 1*), AC5MAb cross-reacted specifically with the AC5 recombinant protein at a molecular mass of ~150 kDa. However, the AC5MAb did not cross-react with lysate from AC6-transfected COS-7 cells (Fig. 1*A*, *lane 2*). The AC5/6 commercial antibody (Cat. No. sc-590; Santa Cruz Biotechnology) only cross-reacted with lysate from AC6-transfected COS-7 cells (Fig. 1*A*, *lane 4*), not from AC5-transfected COS-7 cells (Fig. 1*A*, *lane 3*). To further validate the antibody specificity, Western blot analyses were carried out using membrane preparations from the heart and brain tissues of AC5 KO, WT, and TG mice with cardiac-specific overexpression of AC5. AC5MAb did not cross-react with proteins isolated from AC5 KO heart (Fig. 1*B*) and brain (Fig. 1*C*). The expression of AC5 increased significantly in AC5 TG hearts compared with the WT hearts (Fig. 1*B*), whereas the expression in the brain remained comparable with the WT brains (Fig. 1*C*). Different from the theoretical molecular mass of AC5 (139 kDa), which was calculated using the reported sequence and the ExPasy Server (http://www.expasy.org), AC5MAb cross-reacted with proteins at ~150 kDa in AC5-transfected cells, in the heart and brain, which could be due to differences in *1*) posttranslational modification in AC5 versus AC6 and *2*) apparent molecular mass versus calculated molec-

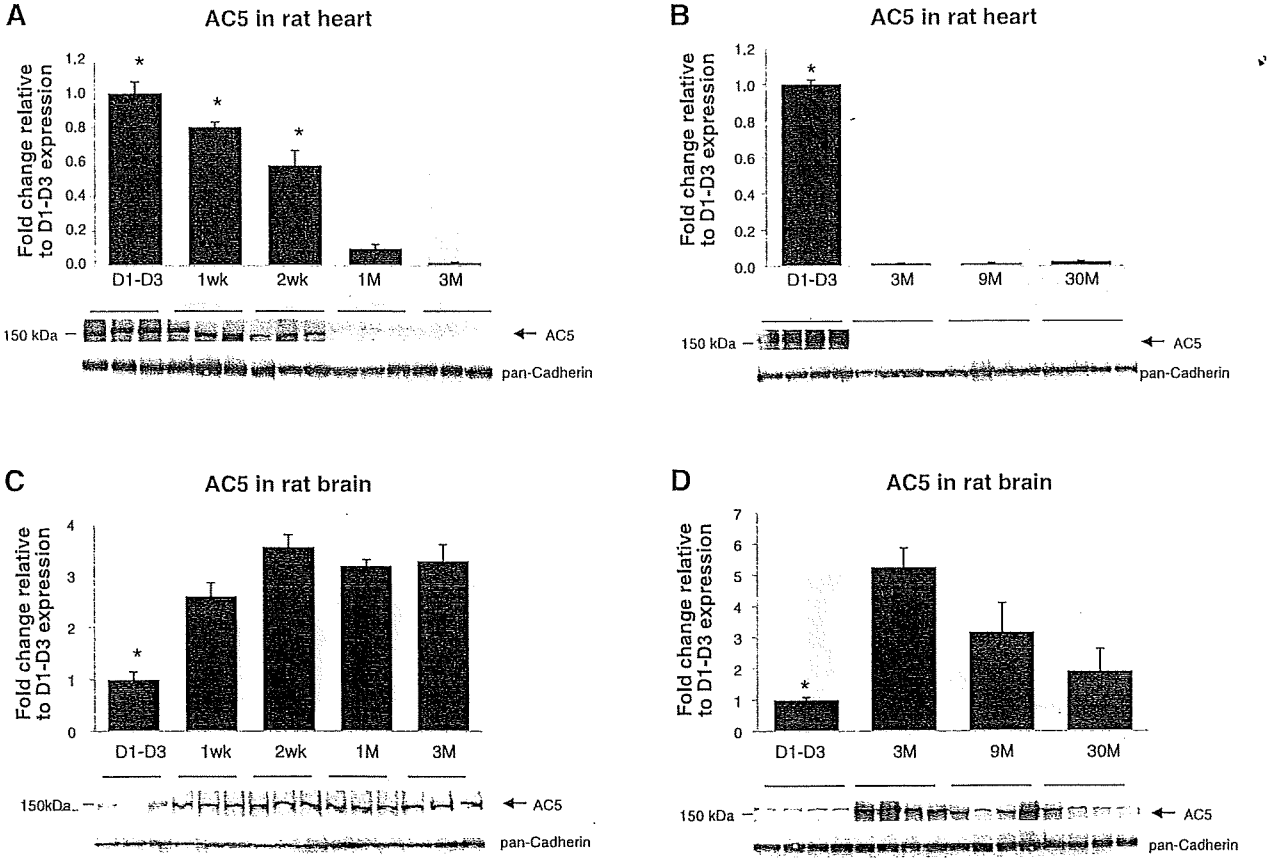

Fig. 5. AC5 protein levels in rat heart and brain tissues. Immunoblotting was performed with AC5MAb using rat heart and brain homogenates. Western blots were run individually for each age group: *D1–D3*, 1 wk, 2 wk, 1 mo, and 3 mo from rat heart (n = 3/age group) (*A*); *D1–D3*, 3 mo, 9 mo, and 30 mo from rat heart (n = 4/age group) (*B*); *D1–D3*, 1 wk, 2 wk, 1 mo, and 3 mo from rat brain (n = 3/age group) (*C*); and *D1–D3*, 3 mo, 9 mo, and 30 mo from rat brain (n = 4/age group) (*D*). AC5 protein was highest in rat neonatal heart (before 2 wk) and lowest in rat neonatal brain (before 1 wk) compared to adult (*$P < 0.05$ vs. other groups). Data are normalized to rat *D1–D3* samples and expressed as means ± SE.

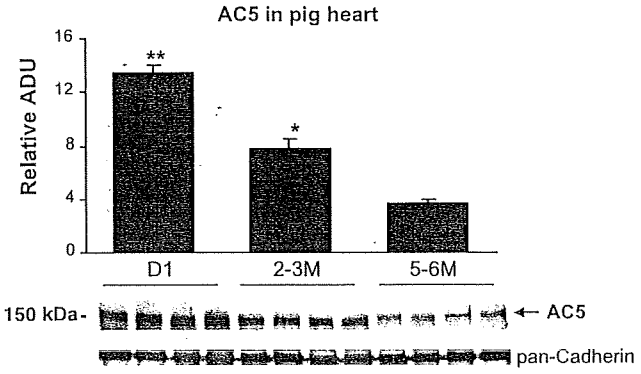

Fig. 6. AC5 expression varies by age in pig hearts. Western blot analysis of AC5 expression in pig hearts showed highest levels in neonatal animals. Equal amounts of membrane preparations (25 μg) were compared between neonatal (*day 1*), young (2 to 3 mo), and adult (5 to 6 mo) pig hearts ($n = 4$). Pan-cadherin was used as a loading control. The level of AC5 protein expression significantly decreased with age. *$P < 0.05$ compared with the adult; **$P < 0.01$. Data are expressed as means ± SE. ADU, arbitrary densitometric units.

ular mass. For example, the reported molecular mass of $G_s\alpha$ is 46 kDa; however, the apparent molecular mass of $G_s\alpha$ is 45 and 52 kDa (24). In addition, the sizing accuracy for SDS-PAGE depends on the protein characteristics such as amino acid sequence, isoelectric point (pI), structure, and hydrophobicity (1). Since these specific protein characteristics can affect migration, it is possible that not all proteins migrate according to their expected molecular masses (3, 14, 18, 28). In fact, pI is quite different for AC5 (pI 6.65) and AC6 (pI 8.16).

The specificity of the AC5MAb was also tested with the AC6 TG mouse heart. The level of AC5 was similar to WT in the AC6 TG mouse heart (Fig. 2*A*). We compared these results with those obtained when using a commercial AC5/6 antibody (Cat. No. sc-590; Santa Cruz Biotechnology). AC protein levels detected by this antibody were not different among WT, AC5 KO, and AC5 TG mouse hearts but significantly increased in the AC6 TG hearts (Fig. 2*B*). These results, together with those in Fig. 1*A*, indicate that this AC5/6 antibody is unlikely to cross-react with the AC5 isoform and reports mainly AC6. We also tested several other commercially available AC5 antibodies; these antibodies were not able to distinguish AC5 expression level in AC5 TG, AC5 KO, and WT mice.

Using the AC5-specific antibody, we examined the tissue distribution of AC5 in organs other than heart and brain. AC5 protein was also found to be expressed in the kidney, lung, liver, stomach, intestine, spleen, skeletal muscle, and vascular tissues (Fig. 3).

Expression of AC5 protein during cardiac development. We next examined the ontogenic expression of AC5 protein during heart development. In the mouse hearts, AC5 protein abundance was highest before 1 wk and then declined to lower levels (Fig. 4*A*), which were indistinguishable from 3 to 24 mo of age (Fig. 4*B*). In contrast, the AC5 protein abundance was relatively low before 1 wk in mouse brain, but it increased significantly after 2 wk (Fig. 4*C*) and remained high from 3 to 24 mo of age in adult brains (Fig. 4*D*). We also analyzed AC5 protein expression in rat heart and brain (Fig. 5) with the similar age patterns of mouse shown in Fig. 4. AC5 protein level was highest before 2 wk and then declined to lower levels in rat heart (Fig. 5*A*), but in rat brain, the AC5 level was low before 1 wk and then increased significantly (Fig. 5*C*). In both old-mouse (24 mo old) and old-rat (30 mo old) brain (Fig. 5*D*), the AC5 level declined compared with the young (3 mo old) brain. These results demonstrated that the mouse and rat heart and brain have the similar AC5 expression patterns. We further analyzed the AC5 protein levels in pig hearts during development. As shown in Fig. 6, the cardiac AC5 protein expression was the highest in 1-day-old pig heart and decreased with age (2 to 3 mo; $P < 0.05$), with the lowest abundance detected at 5 to 6 mo of age ($P < 0.05$ vs. young, and $P < 0.01$ vs. neonates).

To determine whether the AC5 protein expression parallels the mRNA expression during mouse heart development, Northern blot and quantitative PCR analysis were carried out. Northern blot analysis showed that the AC5 mRNA abundance was high in the embryonic (*gestational day 17*) and neonatal hearts, whereas it decreased in the adult (Fig. 7*A*). Quantification of the AC5 transcript confirmed an expression of approximately fivefold higher in the 1-day-old mouse heart compared with the adult heart (Fig. 7*B*).

Expression of AC5 protein in LVH. To evaluate the effect of stress on AC isoforms (AC6 and AC5) in the heart, 4- to 5-mo-old WT mice had transverse aortic banding surgically applied for a 4-wk period. The effects of LVH on AC6 (Fig. 8*A*) and AC5 (Fig. 8*B*) protein content in the heart are shown, with a significant ($P < 0.05$) increase in AC5, as opposed to a significant decrease in AC6 protein levels with LVH.

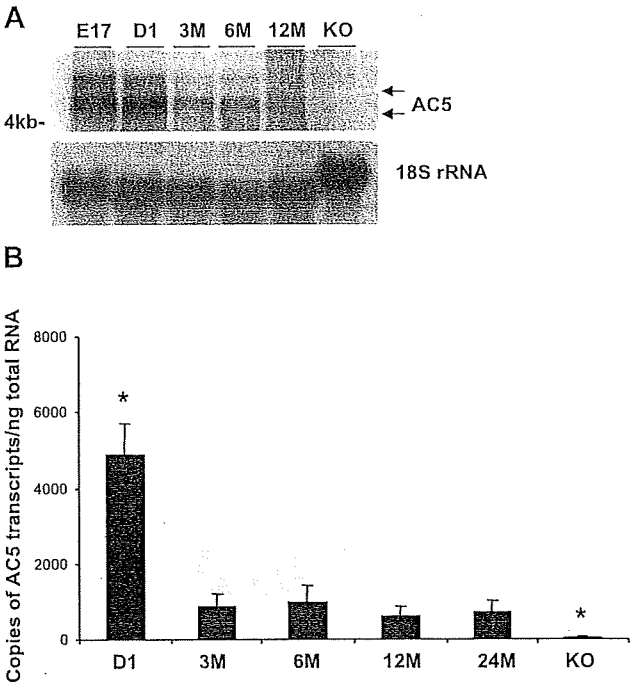

Fig. 7. AC5 mRNA expression in the mouse heart. *A*: Northern blot analysis with total RNA (20 μg) purified from whole WT mouse heart at 6 different stages: *day 17* embryos (E17), *day 1* neonates (D1), 3 mo, 6 mo, and AC5 KO as a negative control. *B*: quantitative real-time RT-PCR with mouse AC5-specific primers and probe (TaqMan). Data are expressed as means ± SE. *$P < 0.05$, significant difference compared with 6-mo mouse hearts. Again, levels were highest in neonatal hearts.

DISCUSSION

In this study, we characterized the AC5 protein expression during heart development in mice, rats, and pigs using an AC isoform-specific mouse monoclonal antibody. Our AC5MAb antibody specifically recognizes AC5 protein (Fig. 1*A*, *lane 1*) and not AC6 protein in the transfected cells or AC6 TG mouse heart. The fact that no AC protein was detected by AC5MAb in the AC5 KO heart and brain tissues (Fig. 1, *B* and *C*) further confirms that our monoclonal antibody is specific for AC5 protein, which is detected at ~150 kDa. One of the antibodies [AC5/6 (c-17)] commonly used to detect AC5/6 changes in AC research could not demonstrate specific changes in AC5 protein expression between AC5 KO, WT, and AC5 TG mouse hearts (Fig. 2*B*). In our study, this commercial antibody did not detect recombinant AC5 protein in the transfected cells (Fig. 1*A*, *lane 3*), indicating that the AC5/6 antibody favorably cross-reacts with the AC6 protein alone. A recent study (27) also showed that the commercial antibody failed to detect AC5 protein in the AC6 KO hearts, further corroborating our results.

Using the AC5MAb, we were able to show the AC5 protein expression profile among various tissues (Fig. 3). Previously, the AC5 transcript was found in the brain, heart, kidney, liver, lung, and testis (4). We also found a significant amount of AC5 expression in skeletal muscle and vessels. Higher expression levels of AC5 in the brain were detected in thalamus, consistent with previous findings in the rat brain where thalamus expression of AC5 mRNA was high throughout the various stages of brain development (19). AC5 mRNA levels were found to be dramatically increased in the adult rat brain, including the striatum.

The AC5 mRNA and protein expression were higher in neonatal compared with adult hearts in mice, rats, and pigs. Interestingly, this pattern for AC5 expression during development differed from that found in the brain, which was lower in neonates (Figs. 4*C* and 5*C*), which was confirmed at both the transcript and the protein levels. Previous studies of AC5 mRNA expression during rat heart development have yielded conflicting information (7, 26, 30). Some studies showed that the expression of the AC5 transcript in the heart increases after birth until cardiac maturation (7, 30), whereas another study (26) showed that the AC5 mRNA decreases from 6 to 24 mo of age in the rat heart. In our study, the expression profile of AC5 during heart development was comparable among mice, rats, and pigs, showing that the neonatal and young hearts have a higher expression than the mature adult heart.

The finding that AC5 protein levels in the heart are highest at birth and decline with age is similar to what is observed with the fetal gene program (13), where increases are observed with LVH. Accordingly, we examined the regulation of AC isoforms in pressure-overload LVH. It would be predicted that AC protein levels would decline with chronic pressure overload, as part of a desensitization program. Indeed, this is what we observed with AC6. Surprisingly, AC5 protein paradoxically increased, further supporting the concept that AC5 behaves like other fetal genes, e.g., atrial natriuretic peptide (2, 8, 15).

In summary, the new AC5 antibody developed in the present investigation represents a novel tool for a proper understanding of the tissue distribution of AC5 and of the ontogenic regulation of AC5 expression, which may be useful for further studies of AC5 signaling. In addition, the availability of a novel type 5 AC antibody will provide new insight into the pathogenesis of disease states. One example, from the current investigation, demonstrating a paradoxical upregulation of AC5 with pressure-overload LVH and its decline with ontogenic development is similar to that of fetal type genes, commonly used markers of cardiac hypertrophy.

ACKNOWLEDGMENTS

We thank Lauren Danridge for patience and help with the manuscript.

GRANTS

This work was supported in part by National Institutes of Health Grants HL-069020, AG-023137, AG-028854, AG-014121, HL-095888, HL-033107, HL-059139, HL-069752, HL-093481, and GM-69861.

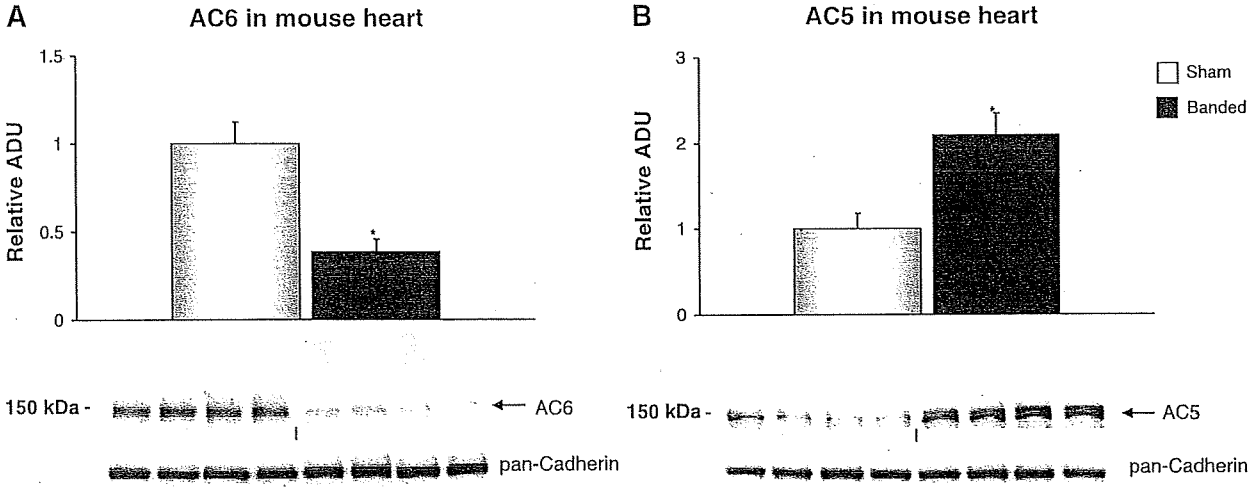

Fig. 8. AC isoform levels in mouse hearts with 4 wk of aortic banding. AC isoform protein levels were detected with immunoblotting using membrane preparations from sham-operated (n = 7) and 4-wk aortic-banded mice (n = 8). AC6 protein levels fell (*A*), and AC5 protein levels rose (*B*). The loading control is shown using pan-cadherin antibody. Data are expressed as means ± SE. *$P < 0.05$.

REFERENCES

1. **Agilent Technologies.** Differences and similarities between the Protein 200 assay and SDS-PAGE: Technical Note, 2001 (http://www.chem.agilent.com/Library/technicaloverviews/Public/59883160.pdf).
2. **Bloch KD, Seidman JG, Naftilan JD, Fallon JT, Seidman CE.** Neonatal atria and ventricles secrete atrial natriuretic factor via tissue-specific secretory pathways. *Cell* 47: 695–702, 1986.
3. **Carlotti F, Zaldumbide A, Charif H, de Koning EJ, Luider TM, Hoeben RC.** The 45-kDa form of Pdx-1 does not result from post-translational modifications. *Biochem Biophys Res Commun* 370: 225–229, 2008.
4. **Defer N, Best-Belpomme M, Hanoune J.** Tissue specificity and physiological relevance of various isoforms of adenylyl cyclase. *Am J Physiol Renal Physiol* 279: F400–F416, 2000.
5. **Depre C, Shipley GL, Chen W, Han Q, Doenst T, Moore ML, Stepkowski S, Davies PJ, Taegtmeyer H.** Unloaded heart in vivo replicates fetal gene expression of cardiac hypertrophy. *Nat Med* 4: 1269–1275, 1998.
6. **Dessauer CW, Gilman AG.** The catalytic mechanism of mammalian adenylyl cyclase. Equilibrium binding and kinetic analysis of P-site inhibition. *J Biol Chem* 272: 27787–27795, 1997.
7. **Espinasse I, Iourgenko V, Defer N, Samson F, Hanoune J, Mercadier JJ.** Type V, but not type VI, adenylyl cyclase mRNA accumulates in the rat heart during ontogenic development. Correlation with increased global adenylyl cyclase activity. *J Mol Cell Cardiol* 27: 1789–1795, 1995.
8. **Gu J, D'Andrea M, Seethapathy M.** Atrial natriuretic peptide and its messenger ribonucleic acid in overloaded and overload-released ventricles of rat. *Endocrinology* 125: 2066–2074, 1989.
9. **Huang C, Hepler JR, Chen LT, Gilman AG, Anderson RG, Mumby SM.** Organization of G proteins and adenylyl cyclase at the plasma membrane. *Mol Biol Cell* 8: 2365–2378, 1997.
10. **Ishikawa Y, Homcy CJ.** The adenylyl cyclases as integrators of transmembrane signal transduction. *Circ Res* 80: 297–304, 1997.
11. **Ishikawa Y, Katsushika S, Chen L, Halnon NJ, Kawabe J, Homcy CJ.** Isolation and characterization of a novel cardiac adenylylcyclase cDNA. *J Biol Chem* 267: 13553–13557, 1992.
12. **Iyengar R.** Molecular and functional diversity of mammalian Gs-stimulated adenylyl cyclases. *FASEB J* 7: 768–775, 1993.
13. **Izumo S, Nadal-Ginard B, Mahdavi V.** Protooncogene induction and reprogramming of cardiac gene expression produced by pressure overload. *Proc Natl Acad Sci USA* 85: 339–343, 1988.
14. **Jassen AK, Brown JM, Panas HN, Miller GM, Xiao D, Madras BK.** Variants of the primate vesicular monoamine transporter-2. *Brain Res Mol Brain Res* 139: 251–257, 2005.
15. **Knowlton KU, Rockman HA, Itani M, Vovan A, Seidman CE, Chien KR.** Divergent pathways mediate the induction of ANF transgenes in neonatal and hypertrophic ventricular myocardium. *J Clin Invest* 96: 1311–1318, 1995.
16. **Laemmli UK.** Cleavage of structural proteins during the assembly of the head of bacteriophage T4. *Nature* 227: 680–685, 1970.
17. **Lane RD, Crissman RS, Ginn S.** High efficiency fusion procedure for producing monoclonal antibodies against weak immunogens. *Methods Enzymol* 121: 183–192, 1986.
18. **Li LB, Chen N, Ramamoorthy S, Chi L, Cui XN, Wang LC, Reith ME.** The role of *N*-glycosylation in function and surface trafficking of the human dopamine transporter. *J Biol Chem* 279: 21012–21020, 2004.
19. **Matsuoka I, Suzuki Y, Defer N, Nakanishi H, Hanoune J.** Differential expression of type I, II, and V adenylyl cyclase gene in the postnatal developing rat brain. *J Neurochem* 68: 498–506, 1997.
20. **Okumura S, Kawabe J, Yatani A, Takagi G, Lee MC, Hong C, Liu J, Takagi I, Sadoshima J, Vatner DE, Vatner SF, Ishikawa Y.** Type 5 adenylyl cyclase disruption alters not only sympathetic but also parasympathetic and calcium-mediated cardiac regulation. *Circ Res* 93: 364–371, 2003.
21. **Okumura S, Takagi G, Kawabe J, Yang G, Lee MC, Hong C, Liu J, Vatner DE, Sadoshima J, Vatner SF, Ishikawa Y.** Disruption of type 5 adenylyl cyclase gene preserves cardiac function against pressure overload. *Proc Natl Acad Sci USA* 100: 9986–9990, 2003.
22. **Okumura S, Vatner DE, Kurotani R, Bai Y, Gao S, Yuan Z, Iwatsubo K, Ulucan C, Kawabe J, Ghosh K, Vatner SF, Ishikawa Y.** Disruption of type 5 adenylyl cyclase enhances desensitization of cyclic adenosine monophosphate signal and increases Akt signal with chronic catecholamine stress. *Circulation* 116: 1776–1783, 2007.
23. **Phan HM, Gao MH, Lai NC, Tang T, Hammond HK.** New signaling pathways associated with increased cardiac adenylyl cyclase 6 expression: implications for possible congestive heart failure therapy. *Trends Cardiovasc Med* 17: 215–221, 2007.
24. **Robishaw JD, Smigel MD, Gilman AG.** Molecular basis for two forms of the G protein that stimulates adenylate cyclase. *J Biol Chem* 261: 9587–9590, 1986.
25. **Sadoshima J, Montagne O, Wang Q, Yang G, Warden J, Liu J, Takagi G, Karoor V, Hong C, Johnson GL, Vatner DE, Vatner SF.** The MEKK1-JNK pathway plays a protective role in pressure overload but does not mediate cardiac hypertrophy. *J Clin Invest* 110: 271–279, 2002.
26. **Scarpace PJ, Matheny M, Tumer N.** Myocardial adenylyl cyclase type V and VI mRNA: differential regulation with age. *J Cardiovasc Pharmacol* 27: 86–90, 1996.
27. **Tang T, Gao MH, Lai NC, Firth AL, Takahashi T, Guo T, Yuan JX, Roth DM, Hammond HK.** Adenylyl cyclase type 6 deletion decreases left ventricular function via impaired calcium handling. *Circulation* 117: 61–69, 2008.
28. **Tate CG, Blakely RD.** The effect of *N*-linked glycosylation on activity of the Na^+- and Cl^--dependent serotonin transporter expressed using recombinant baculovirus in insect cells. *J Biol Chem* 269: 26303–26310, 1994.
29. **Tesmer JJ, Sunahara RK, Gilman AG, Sprang SR.** Crystal structure of the catalytic domains of adenylyl cyclase in a complex with Gsalpha. GTPgammaS. *Science* 278: 1907–1916, 1997.
30. **Tobise K, Ishikawa Y, Holmer SR, Im MJ, Newell JB, Yoshie H, Fujita M, Susannie EE, Homcy CJ.** Changes in type VI adenylyl cyclase isoform expression correlate with a decreased capacity for cAMP generation in the aging ventricle. *Circ Res* 74: 596–603, 1994.
31. **Wang T, Brown MJ.** Differential expression of adenylyl cyclase subtypes in human cardiovascular system. *Mol Cell Endocrinol* 223: 55–62, 2004.
32. **Yan L, Vatner DE, O'Connor JP, Ivessa A, Ge H, Chen W, Hirotani S, Ishikawa Y, Sadoshima J, Vatner SF.** Type 5 adenylyl cyclase disruption increases longevity and protects against stress. *Cell* 130: 247–258, 2007.

Am J Physiol Cell Physiol 297: C802–C813, 2009.
First published August 5, 2009; doi:10.1152/ajpcell.00129.2009.

Epac increases melanoma cell migration by a heparan sulfate-related mechanism

Erdene Baljinnyam,[1]* Kousaku Iwatsubo,[1]* Reiko Kurotani,[3] Xu Wang,[1] Coskun Ulucan,[1] Mizuka Iwatsubo,[1] David Lagunoff,[1] and Yoshihiro Ishikawa[1,2,3]

[1]*Department of Cell Biology and Molecular Medicine, and* [2]*Department of Medicine (Cardiology), New Jersey Medical School-University of Medicine and Dentistry of New Jersey, Newark, New Jersey;* [3]*Cardiovascular Research Institute, Yokohama City University Graduate School of Medicine, Yokohama, Japan*

Submitted 23 March 2009; accepted in final form 3 August 2009

Baljinnyam E, Iwatsubo K, Kurotani R, Wang X, Ulucan C, Iwatsubo M, Lagunoff D, Ishikawa Y. Epac increases melanoma cell migration by a heparan sulfate-related mechanism. *Am J Physiol Cell Physiol* 297: C802–C813, 2009. First published August 5, 2009; doi:10.1152/ajpcell.00129.2009.—Melanoma, the most malignant form of human skin cancer, has a poor prognosis due to its strong metastatic ability. It was recently demonstrated that Epac, an effector molecule of cAMP, is involved in regulating cell migration; however, the role of Epac in melanoma cell migration remains unclear. We thus examined whether Epac regulates cell migration and metastasis of melanoma. Epac activation, by either specific agonist or overexpression of Epac, increased melanoma cell migration. Deletion of endogenous Epac with small interfering RNA decreased basal melanoma cell migration. These data suggested a major role of Epac in melanoma cell migration. Epac-induced cell migration was mediated by translocation of syndecan-2, a cell-surface heparan sulfate proteoglycan, to lipid rafts. This syndecan-2 translocation was regulated by tubulin polymerization via the Epac/phosphoinositol-3 kinase pathway. Epac-induced cell migration was also regulated by the production of heparan sulfate, a major extracellular matrix. Epac-induced heparan sulfate production was attributable to the increased expression of *N*-deacetylase/*N*-sulfotransferase-1 (NDST-1) accompanied by an increased NDST-1 translation rate. Finally, Epac overexpression enhanced lung colonization of melanoma cells in mice. Taken together, these data indicate that Epac regulates melanoma cell migration/metastasis mostly via syndecan-2 translocation and heparan sulfate production.

metastasis; phosphoinositol-3 kinase; *N*-deacetylase/*N*-sulfotransferase-1

MELANOMA IS A MAJOR CANCER worldwide including the United States. The median life span of patients with advanced stage melanoma is less than a year because there are no effective therapies once the tumor has spread to vital organs (5). The process of tumor cell metastasis is conventionally understood as the migration of individual cells that detach from the primary tumor, enter lymphatic vessels or the bloodstream, attach to endothelial cells, and undergo transendothelial extravasation and proliferate in organs. Despite numerous efforts in the research field, the understanding and controlling of melanoma cell migration/metastasis has been unsuccessful.

In addition to the conventional cAMP signaling pathway through protein kinase A (PKA), a new, PKA-independent signaling pathway has been established with the discovery of the exchange protein directly activated by cAMP (Epac), a guanine nucleotide exchange factor (12). Two isoforms of Epac, Epac1 and Epac2, were shown to mediate cAMP signaling to activate a small-molecular-weight G protein Rap1 and to regulate cellular functions, including secretion, Ca^{2+} signaling, proliferation, and apoptosis (6). Several reports also indicate the involvement of Epac in regulating cell migration (16, 28); however, the molecular mechanisms that lead to increased cell migration through Epacs remain unknown.

Molecular events associated with cell migration are influenced by interactions between cell surface molecules and the extracellular matrix (ECM) components (4). Syndecan-2, a member of the cell surface heparan sulfate (HS) proteoglycans (HSPGs), regulates cell migration via binding to extracellular HS (19, 45). HS is a major ECM component and regulates multiple cellular functions including migration (14). These reports suggested that the coordination of syndecan-2 and HS plays a role in cell migration; however, little is known about the key molecule that regulates such coordination. In this report, we demonstrate that Epac increases melanoma cell migration using two human melanoma cell lines: SK-Mel-2, which was derived from regional metastasis, and SK-Mel-24, which was derived from lymph node metastasis; both cell lines show potent migratory ability (16, 38). We also demonstrated that syndecan-2 translocation and HS production are involved in Epac-induced cell migration. In vivo studies have shown that Epac increases melanoma metastasis to the lung in mice. We thus propose a mechanism of regulating melanoma cell migration/metastasis, which is related to HS and its core binding protein.

MATERIALS AND METHODS

Materials. Wortmannin, nocodazole, cycloheximide, and cyclodextrin were purchased from Sigma Aldrich. PD-98059 and LY-294002 reagents were purchased from EMD Biosciences. 8-(4-methoxyphenylthio)-2'-*O*-methyladenosine-3',5'-cAMP (8-pMeOPT-2-*O*-Me-cAMP) and N^6-monobutyryl-cAMP (6-MB-cAMP) were purchased from Axxora. BD adeno-X expression system, BD-Adeno-X virus purification kit, and rapid titer kit were purchased from Clontech. MEM, FBS, trypsin-EDTA, Lipofectamine 2000, and penicillin-streptomycin were purchased from Invitrogen. Antibodies for phospho-glycogen synthetic kinase 3-β (GSK3β), GSK3β, phospho-Akt, and Akt were purchased from Cell Signaling. Antibodies for Epac1, Epac2, PKA (α-catalytic subunit), cAMP-response element-binding protein (CREB), phospho-CREB, and Rap1 were purchased from Santa Cruz. Anti-*N*-deacetylase/*N*-sulfotransferase-1 (NDST1) antibody was purchased from Abnova. Anti-syndecan-1 antibody was purchased from Invitrogen. Anti-anti-α-tubulin antibody was purchased from Abcam. Anti-HS antibody was purchased from Kamiya Biomedical.

* E. Baljinnyam and K. Iwatsubo contributed equally to this work.
Address for reprint requests and other correspondence: K. Iwatsubo, G-653, MSB, 185 S. Orange Ave., Newark, NJ 07103 (E-mail: iwatsuko@umdnj.edu) or Y. Ishikawa, 3-9 Fukuura Kanazawa-ku, Yokohama, 236-0004, Japan.

Cell culture. SK-Mel-2 and SK-Mel-24 (ATCC) cell lines were cultured in Eagle's MEM supplemented with 10% fetal bovine serum at 37°C-5% CO_2. HEMA-LP human melanocytes (Cascade Biologics) were maintained in Medium 254 with Human Melanocyte Growth Supplement (Cascade Biologics).

Adenoviral overexpression. Recombinant adenoviruses containing human LacZ, Epac1, or Epac2 were constructed (Adeno-X Expression System, Clontech). Human Epac1 and Epac2 cDNA were kindly provided by Dr. J. L. Bos (University Medical Center, Utrecht, The Netherlands). Adenovirus of PKA α-subunit was purchased from Vector Biolabs. The corresponding encoding sequence was cloned into pShuttle2 (Clontech) to obtain a mammalian expression cassette, which was then excised and ligated into BD Adeno-X Viral DNA. The recombinant vector was introduced into human embryonic kidney cells (HEK-293) to recover infectious adenovirus. Viruses were propagated in HEK-293 cells and purified by BD Adeno-X Virus Purification Kits. Viral titer was determined by Adeno-X Rapid Titer Kit (Clontech). As a control study, adenovirus vector harboring LacZ was used at the same multiplicity of infection. Cells were infected with adenovirus for 24 h and subjected to each experiment. In some experiments (for HS production and NDST-1 expression; see Fig. 5, *B–H*), cells were further incubated for 48 h in medium without adenovirus.

Quantitative real-time PCR. Quantitative real-time PCR (qPCR) was performed as we previously described (41). Total RNA was extracted using RNAeasy kit (QIAGEN), and then first-strand cDNA was synthesized using the Taqman RT reagents (Applied Biosystems). Real-time PCR was then carried out on a DNA Engine Opticon 2 system (MJ Research) using the SYBR Green qPCR kit (Bio-Rad). Three sets of predesigned primer mixes for each gene of interest were optimized. Specific oligonucleotide primers were used in this study: Epac1 [Hs_RAPGEF3_1_SG (QT00003381, QIAGEN)], Epac2 (Hs00199754-m1RAPGEF4, ABI), and NDST-1 [Hs_NDST1_1SG Quantitect Primer Assay(QT01002638, QIAGEN)].

Migration assay and invasion assay. Migration assay was performed as we previously described by using the Boyden chambers (44) (pore size 8 μm, BD Biosciences). The upper chamber's polycarbonate insert film parts were coated by 75 μl fibronectin (50 μg/ml in PBS, BD Biosciences). Cultured cells were detached and the number of the cells was adjusted to 1×10^3 cells/μl of media. One-hundred microliters of the cell suspension were applied to the center of the upper chamber and then attached to the lower chamber. Thereafter, the cells were incubated in CO_2 incubator at 37°C for 3 h unless specified. After fixation with 10% formalin neutral solution, cells were stained with Diff-Quick kit (Dade Behring). After mechanical removal of the cells on the upper surface of the membrane with a cotton swab, the cells that migrated onto the lower surface of the membrane were counted. Pictures were taken with a microscope followed by counting migrated cells with Image J software in randomly chosen 10 fields. Invasion assay was performed by using Boyden chambers as described above, except that Matrigel (BD Biosciences) was used as coating.

Time-lapse videomicroscopy. Analysis of cell motility using time-lapse videomicroscopy was performed as we previously demonstrated (37). SK-Mel-2 cells overexpressing either LacZ or Epac1 were subjected to time-lapse video recording. Frames from the recording were digitized, and cell locations were identified at 30-min intervals by using either the centroids or nuclei. The speed of cell movement was determined for distances between their successive positions.

Western blot analysis. Western blot analysis was performed as we described previously (20). Cells were lysed and sonicated in lysis buffer containing 25 mM Tris·HCl (pH 7.5), 150 mM NaCl, 5 mM $MgCl_2$, 1% Nonidet P-40, 1 mM dithiothreitol, 5% glycerol, phosphatase inhibitor (Sigma), protease inhibitor cocktail (Sigma), and 1 mM NaF. Equal amounts of protein (20–90 μg) were subjected to SDS-PAGE. After protein separation by electrophoresis, samples were transferred to Millipore Immobilon-P membrane, and immunoblotting with antibodies was performed. Signal intensities of the bands were quantified with Image J software (NIH).

Immunoprecipitation. Immunoprecipitation was performed as previously described (34). Cells were lysed in RIPA buffer containing 10 μg/ml aprotinin, 10 μg/ml leupeptin, 1 mM sodium orthovanadate, and 1 mM phenylmethylsulfonyl fluoride (PMSF). Immunoprecipitations were performed overnight at 4°C using antibodies with protein A-Sepharose. Samples were then subjected to Western blot analysis. For syndecan-2 immunoprecipitation, beads for immunoprecipitation were subjected to heparitinase treatment for 4 h at 37°C to separate syndecan-2 from HS chains.

Transfection with siRNA. Epac1 small interfering RNA (siRNA) (Ambion), Epac1 siRNA (Ambion), syndecan-2 siRNA (Ambion), and NDST-1 siRNA (Qiagen) were transfected into subconfluent SK-Mel-2 cells using Lipofectamine 2000 (Invitrogen). A pool of double-stranded siRNAs containing equal parts of the following antisense sequences was used: 5′-AUCACUGUAUACCGGUUCC-3′ (Epac1), 5′-CUCUGGACUCUCUACAUCC-3′ (syndecan-2), and 5′-UUUAUUAGCAGUUAGUUCG-3′ (NDST-1). The corresponding nontargeting siRNA silencer negative control no. 2 siRNA (AM4613, Ambion) was used as a negative control. Twenty-four hours later, the medium containing siRNA was changed to fresh medium and incubated for 72 h. When siRNA transfection was combined with adenoviral infection, siRNA transfection followed the adenoviral infection.

HS ELISA. HS content was determined as previously described with HS ELISA kit (Seikagaku) (36). Cells were collected and disrupted by sonication followed by centrifugation at 14,000 rpm for 10 min. The supernatants were collected and diluted six times and incubated for 18 h at 4°C in the plates coated with HS antibody (20 μg/diluted sample). The secondary reaction with horseradish peroxidase-conjugated streptavidin-biotinylated antibody was carried out for 1 h at room temperature. After color development and stop reaction, OD was measured at 350/630 nm.

Tubulin polymerization assay. Tubulin polymerization assay was performed as we previously described (23). Cells were washed gently twice with 2 ml prewarmed PBS/wash. After the addition of 400 μl of microtubule-stabilizing buffer (MSB) containing 100 mM Tris·HCl (pH 6.75), 1 mM EGTA, 1 mM $MgCl_2$, 2 M glycerol, 0.1% Triton-X 100, 200 μM PMSF, 10 U/ml egg white trypsin inhibitor (ETI), and 20 μg/ml leupeptin, the cells were incubated for 15 min at 37°C. The cells were then incubated again with 400 μl MSB containing 0.1% Triton-X for 15 min at 37°C. Eighty microliters of 72% trichloroacetic acid and 80 μl of 0.15% DOC were added to total 800 μl of the collected samples. The mixtures were incubated on ice for 10 min and centrifuged at 14,000 rpm for 15 min. The pellets were resuspended with 100 μl of 100 mM NaOH and subjected to SDS-PAGE as a monomeric tubulin fraction. The remaining cells were resuspended with 70 μl lysis buffer [50 mM Tris·HCl (pH 6.8), 1 mM EDTA, 1% SDS, 10% glycerol, and 1 mM PMSF] and homogenated using a sonicator (1 s, once) and subjected for SDS-PAGE as a polymeric tubulin fraction.

[^{35}S]methionine pulse-labeling assay. [^{35}S]Methionine pulse-labeling assay was performed as previously described (3). The cells were incubated with 100 μCi [^{35}S]methionine for 18 h at 37°C. The cells were then lysed with immunoprecipitation buffer (0.5% Nonidet P-40, 0.5% deoxycholate, 0.1% SDS, and 0.05 M Tris·HCl, pH 7.5) followed by immunoprecipitation with anti-NDST-1 antibody. The amount of radiolabeled NDST-1 precipitate was analyzed by SDS-PAGE followed by autoradiography overnight at 4°C.

Sucrose density gradient centrifugation. Lipid rafts-enriched membrane fractions with sucrose density gradient centrifugation were prepared as we previously described (34). Briefly, cells were homogenated in 2 ml of 500 mM sodium carbonate (pH 11.0) with protease inhibitors (1 μg/ml leupeptin, 0.1 mM PMSF, and 50 U/ml ETI) and lysed by sonication. The lysate was then adjusted to 45% sucrose by mixing with 2 ml of 90% sucrose prepared in 25 mM 2-morpholinoethanesulfonic acid (MES) (pH 6.5) and 0.15 mM NaCl (MBS

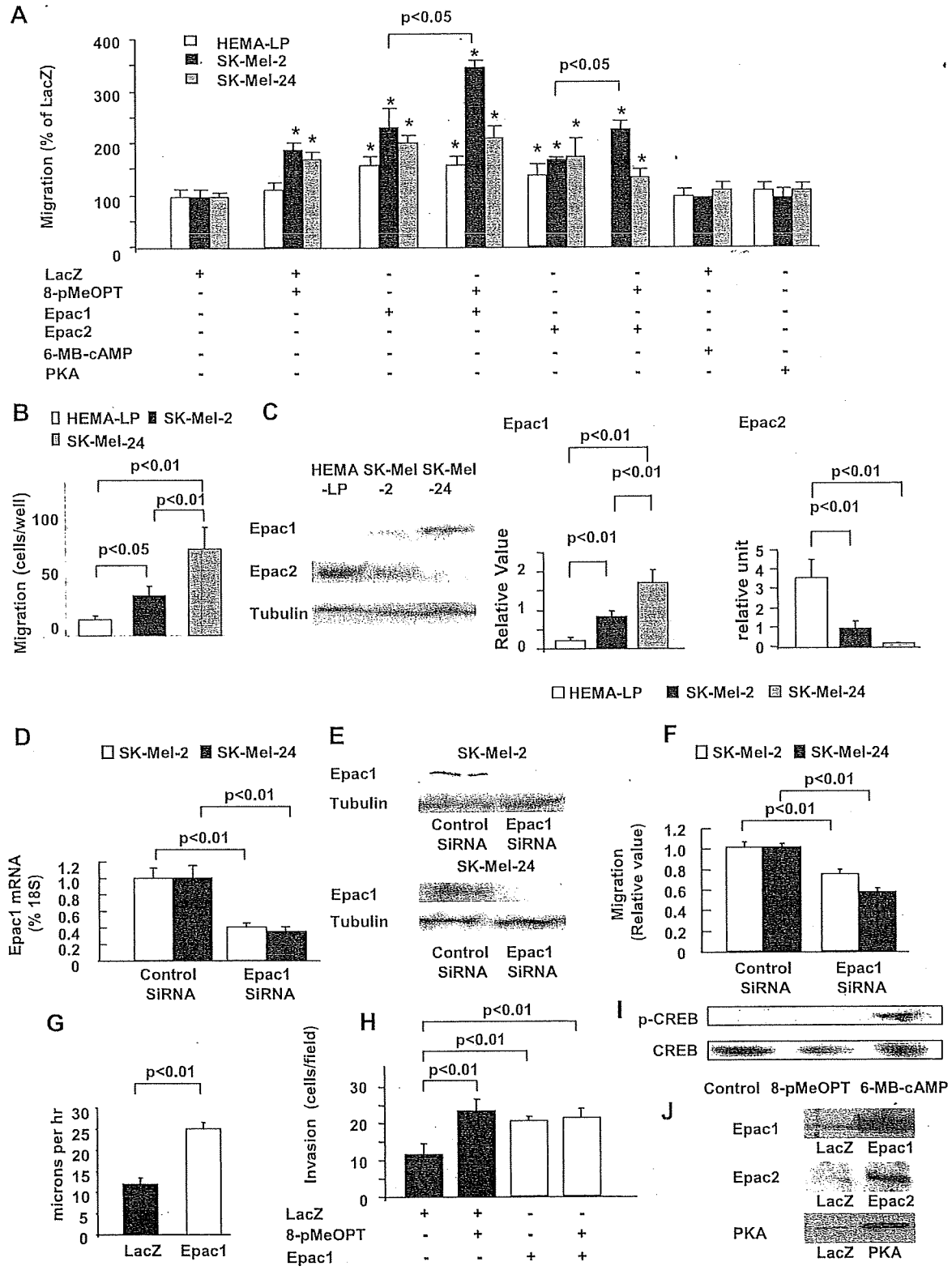

buffer) and placed at the bottom of 5% and 35% discontinuous sucrose gradient (in MBS buffer containing 100 mM sodium carbonate) for an overnight ultracentrifugation (260,000 *g*). Fractions were removed sequentially from the top and designated as *fractions 1* through *13*. Then *fraction 6*, the lipid rafts-enriched fraction, was subjected to immunoprecipitation or Western blot analysis. Flotillin, a lipid raft-associated protein, was used to confirm the existence of lipid rafts in these fractions.

Immunocytochemistry. Immunocytochemistry was performed as we previously described (21). SK-Mel-2 cells cells on glass coverslips were fixed on glass coverslips, washed, and permeabilized with 0.02% Triton-X followed by incubation with primary and secondary antibodies for 30 min at room temperature. Alexa Fluor 488- and 594-conjugated goat anti-rabbit or anti-mouse antibodies (Molecular Probes) were used. The pictures were taken with a digital camera operated on a Nikon Eclipse TE200 or a confocal microscope (Zeiss Axiovert 100M). For mounting media, Prolong-Gold antifade with DAPI (Molecular Probes) was used.

Lung colonization assay. To examine the metastatic potential of melanoma cells, lung colonization assay was performed as described previously (11, 43). In brief, Cloudman S91 melanoma cells (clone M3, European Collection of Cell Cultures) were maintained in Ham's F-10 (Sigma) with 2.5% FCS and 15% normal horse serum. The cells were infected with adenovirus expressing Epac1 or green fluorescent protein (GFP) and incubated for 36 h. The expression of Epac1 was examined by Western blot analysis. The cells were harvested and injected (2×10^6 cells/0.2 ml) into tail veins of BALB/c nude mice (Charles River, male, 6 wk old). Two weeks after the injection, the number of metastatic colonies on the surface of the lungs was counted under a dissection microscope. This study was approved by the Animal Care and Use Committee at Yokohama City University.

Statistical analysis. All results are expressed as means ± SE. Differences in all parameters between experimental groups were analyzed using Student's *t*-test or analysis of variances (ANOVA), followed by post hoc analysis Fischer test for multiple observations. Differences were considered significant when P values were <0.05.

RESULTS

Epac increases migration in melanoma. We examined the effect of target proteins of cAMP, i.e, Epac and PKA, on cell migration in melanocyte (HEMA-LP) and melanoma cell lines (SK-Mel-2 and SK-Mel-24) (Fig. 1*A*). 8-pMeOPT, an Epac-specific agonist, increased cell migration in melanoma cells lines, but not in a melanocyte cell line. By contrast, 6-MB-cAMP, a PKA agonist, did not increase cell migration in any of the cell lines, whereas it increases phosphorylation of CREB (Fig. 1*I*). Adenoviral overexpression of Epac1 and Epac2, but not PKA (Fig. 1*J*), increased melanoma cell migration (Fig. 1*A*). Overexpression of Epacs also increased melanocyte cell migration, suggesting that Epac provides migratory ability.

Basal migration was higher in melanoma cell lines than in melanocytes. Between the two melanoma cell lines, SK-Mel-24 cells showed higher migration than SK-Mel-2 cells (Fig. 1*B*). When we examined the expression of Epacs, protein expression of Epac1 was higher in melanoma cell lines than in melanocytes, and higher in SK-Mel-24 than in SK-Mel-2 cells (Fig. 1*C*, *left*). By contrast, the protein expression of Epac2 was the highest in melanocytes among the cell lines (Fig. 1*C*, *right*). These data suggested the major role of endogenous Epac1 in melanoma cells, but the minor role of Epac2 in melanocytes, in cell migration.

We next examined whether deletion of Epac1 reduces melanoma cell migration. When Epac1 expression was decreased by siRNA (Fig. 1, *D* and *E*), cell migration was decreased (Fig. 1*D*). Video-recorded cell motility was also increased by Epac1 overexpression (Fig. 1*G* and supplemental video). Furthermore, Epac increased melanoma cell invasion (Fig. 1*H*), suggesting that Epac enhances not only cell migration but also invasion.

Epac-induced cell migration is mediated by the translocation of syndecan-2. We investigated changes in cell surface molecules which regulate cell migration. Since HSPGs, such as syndecan-2 and glypicans, play a role in cell migration (19, 45), we examined the changes in localization and the expression of glypicans and syndecan-1, -2, and -4. Using immunocytochemistry, we found that Epac1 overexpression increased a particle size of the syndecan-2 immunofluorescent signal, but not of the other HSPGs (data not shown). We also examined expression changes of HSPGs including syndecan-2, however, Epac1 overexpression did not change the expression of syndecan-2 (Fig. 2*B*) or the expression of the other HSPGs (data not shown). Since syndecan is known to translocate to lipid rafts (40), which serve as platforms for molecules involved in cell migration (26, 30, 32), we hypothesized that such large particle size indicates accumulation of syndecan-2 in lipid rafts. Indeed, immunocytochemistry showed that both Epac agonist and Epac1 overexpression increased colocalization of syndecan-2 with lipid rafts. Cyclodextrin (CXD), a lipid rafts-disrupting agent, decreased such colocalization (Fig. 2*A*). Additionally, in lipid rafts-rich fraction purified from sucrose density gradient centrifugation, syndecan-2 expression was increased by Epac1 overexpression (Fig. 2*C*). These data suggested that Epac increases translocation of syndecan-2 to lipid rafts.

We next examined whether translocation of syndecan-2 to rafts is involved in Epac-induced cell migration. When lipid rafts was disrupted by CXD, basal and Epac-induced cell

Fig. 1. Epac increases melanoma cell migration. *A*: Epac increases melanoma cell migration. Cells were infected with adenovirus harboring LacZ, Epac1, Epac2, and protein kinase A (PKA) followed by the migration assay in the presence or absence of 50 μM 8-(4-methoxyphenylthio)-2'-*O*-methyladenosine-3',5'-cAMP (8-pMeOPT) or 50 μM N^6-monobutyryl-cAMP (6-MB-cAMP). Both 8-pMeOPT and Epac overexpression, but neither 6-MB-cAMP nor PKA overexpression, increased melanoma cell migration. $*P < 0.01$ vs. LacZ. $n = 4$. *B*: basal migration assay in melanocytes and melanoma cell lines is shown. Basal migration was higher in melanoma cell lines than in melanocytes and in SK-Mel-24 cells than in SK-Mel-2 cells. $n = 4$. *C*: immunoblots for Epac1 and Epac2. Epac1 protein expression was more abundant in melanoma cell lines than in melanocytes and in SK-Mel-24 cells than in SK-Mel-2 cells. Epac2 protein expression was more abundant in melanocytes than in melanoma cell lines. Bar graphs show densitometric analyses of the blots. $n = 4$. *D*: quantitative real-time PCR (qPCR) showed that Epac1 small interfering RNA (siRNA) decreased mRNA expression in SK-Mel-2 cells or SK-Mel-24 cells are shown. $n = 4$. *E*: immunoblots showed that Epac1 siRNA decreased Epac1 protein expression in both SK-Mel-2 and SK-Mel-24 cells. *F*: Epac1 siRNA decreased basal cell migration in SK-Mel-2 cells or SK-Mel-24 cells. $*P < 0.01$ vs. control siRNA. $n = 4$. *G*: video-recorded analysis showed that SK-Mel-2 cells overexpressing Epac1 significantly increased cell motility. $n = 10$. Supplementary video files; video-recorded cell motility is shown. 1 second in video approximately corresponds to 1 h recording. *H*: invasion assay showed that both 8-pMeOPT and Epac1 overexpression increased invasion of SK-Mel-2 cells. $n = 4$. *I*: immunoblot showed that 6-MB-cAMP, but not 8-pMeOPT, increased phosphorylation of cAMP-response element-binding protein (CREB). *J*: immunoblot showed overexpression of Epac1, Epac2, and PKA with adenoviral infection in SK-Mel-2.

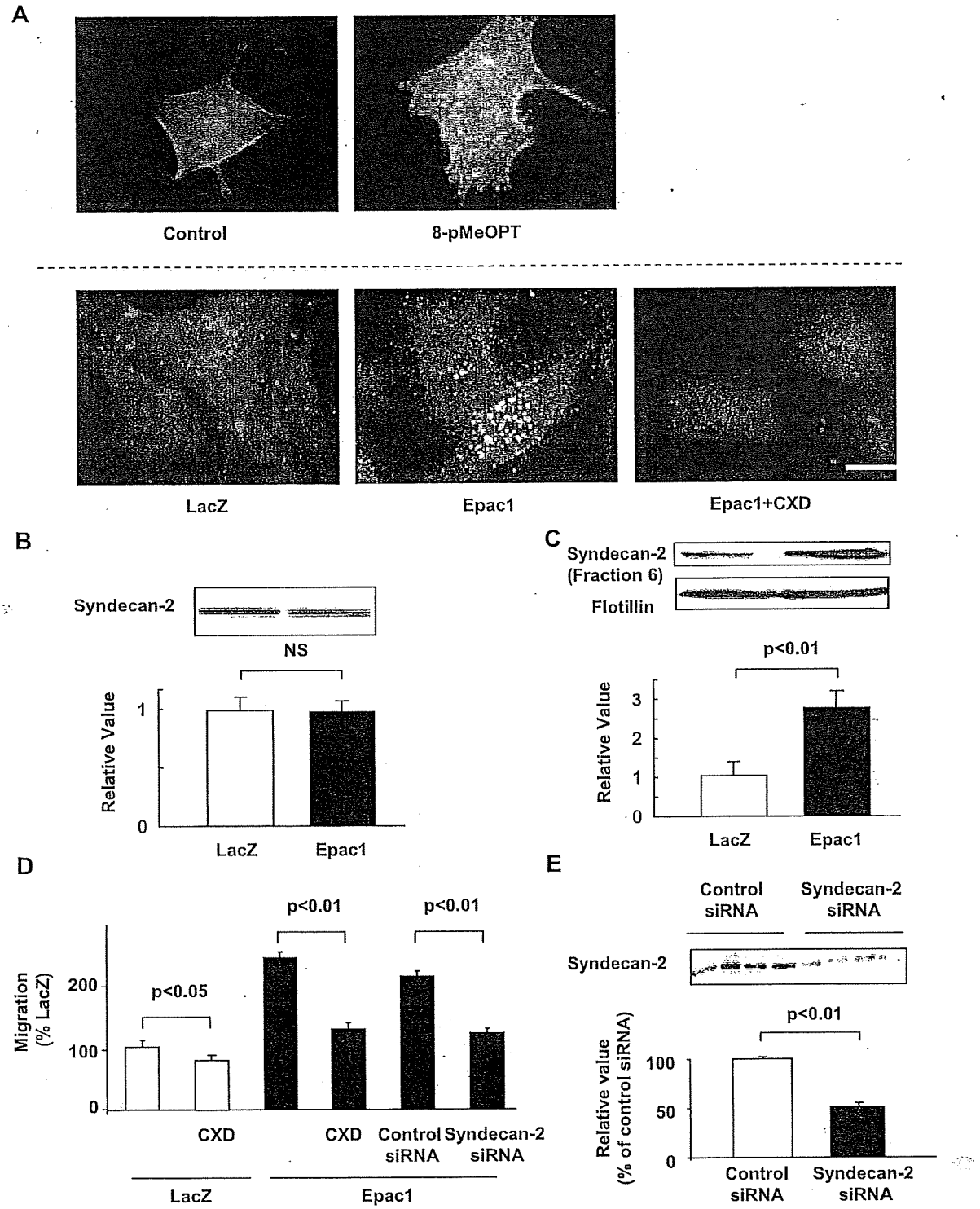

Fig. 2. Epac activates syndecan-2 translocation into rafts in SK-Mel-2. *A*: immunocytochemistry for syndecan-2 (red) and FLAER (green) is shown. *Top*, cells were incubated in the presence or absence of 50 μM 8-pMeOPT for 15 min. 8-pMeOPT induced colocalization of syndecan-2 with lipid rafts (yellow). *Bottom*, cells overexpressing LacZ or Epac1 were incubated in the presence or absence of 10 μg/ml CXD. Epac1 overexpression increased colocalization of syndecan-2 with lipid rafts (yellow). CXD decreased such colocalization. *B*: immunoblot showed that syndecan-2 expression was not changed by Epac1 overexpression. $n = 4$. *C*: immunoblot showed that Epac1 overexpression increased syndecan-2 expression in rafts-rich fraction. Flotillin was used for a marker of lipid rafts. $n = 4$. *D*: migration assay showed that CXD (10 μg/ml) decreased basal and Epac1 overexpression-induced cell migration. Syndecan-2 siRNA also inhibited Epac1 overexpression-induced cell migration. $n = 4$. *E*: immunoblot showed decreased syndecan-2 expression with siRNA. $n = 4$.

migration was inhibited (Fig. 2*D*), suggesting that lipid rafts are necessary for Epac-induced cell migration. We also examined the effect of deletion of syndecan-2 on Epac-induced cell migration. When syndecan-2 expression was decreased with siRNA (Fig. 2*E*), Epac-induced cell migration was inhibited (Fig. 2*D*). These data suggested that the translocation of syndecan-2 to lipid rafts is involved in Epac-induced cell migration.

Epac translocates syndecan-2 to lipid rafts by tubulin polymerization. We investigated the mechanism by which Epac regulates syndecan-2 translocation. Since tubulin polymerization is known to mediate intracellular molecule transport (15), and syndecan-2 has a tubulin-binding motif in its intracellular domain (8), we hypothesized that tubulin polymerization mediates Epac-induced translocation of syndecan-2. In melanoma cells, indeed, syndecan-2 is physically bound to tubulin (Fig. 3*A*). Such binding was not augmented by Epac1 overexpression, suggesting that Epac mediates syndecan-2 translocation not by enhancing the physical interaction between syndecan-2 and tubulin. We thus examined whether Epac increases tubulin polymerization, and this polymerization leads to syndecan-2 translocation. Epac1 overexpression increased polymer form of tubulin (Fig. 3*B*). In support, immunocytochemistry showed increased tubulin fine structure (Fig. 3*C*), which is known to reflect tubulin polymerization (17). These data suggested that Epac increases tubulin polymerization.

We next examined whether inhibition of tubulin polymerization prevents syndecan-2 translocation to lipid rafts. Immunocytochemistry showed that nocodazole (NCD), a tubulin polymerization inhibitor, decreased the colocalization of syndecan-2 with lipid rafts (Fig. 3*D*). NCD also decreased the expression of syndecan-2 in the lipid rafts-rich fraction (Fig. 3*E*). These data suggested that tubulin polymerization mediates Epac-induced syndecan-2 translocation to lipid rafts. Furthermore, NCD inhibited Epac-induced cell migration (Fig. 3*F*), supporting the concept that tubulin polymerization is involved in Epac-induced cell migration.

Epac mediates tubulin polymerization via PI3 kinase. We next explored the mechanism by which Epac increases tubulin polymerization. Although a recent study demonstrated a direct binding of Epac to tubulin (29), this was not the case, at least, in melanoma cells; neither immunocytochemical studies nor immunoprecipitation assays showed association of Epac1 with tubulin in our study (data not shown). It is well known that the phosphoinositol-3 kinase (PI3K) regulates tubulin polymerization via the Akt/GSK3β pathway (48, 49). Also, a report demonstrated that Epac activates PI3K (7, 22, 31). Therefore, we hypothesized that Epac. increases tubulin polymerization via PI3 kinase. Wortmannin, a PI3K inhibitor, inhibited Epac-induced tubulin polymerization (Fig. 4*A*). Wortmannin also inhibited Epac-induced phosphorylation of Akt (Fig. 4*B*) and GSK3β (Fig. 4*C*). These data suggested that the PI3K/Akt/GSK3β pathway is involved in Epac-induced tubulin polymerization. Wortmannin also decreased Epac-induced syndecan-2 localization in lipid rafts (Fig. 4, *D* and *E*) and migration (Fig. 4*F*), further supporting the involvement of PI3K in Epac-induced cell migration.

Epac increases melanoma cell migration via HS production. Since lipid rafts serve as a platform for the binding of syndecans to the ECMs (24), the translocation of syndecan-2 is likely to augment the binding between melanoma cells and ECMs via syndecan-2. Because HS is a major component among syndecan-2-bound ECMs (19), we examined whether translocation of syndecan-2 augments its binding to extracellular HS. We found that the glycanated form of syndecan-2, which reflects the HS-bound form of syndecan-2 (35), was increased by Epac1 overexpression (Fig. 5*A*). These data indicate the possibility that Epac increases the amount of extracellular HS itself. We thus examined whether Epac increases HS production in melanoma cells. Interestingly, Epac1 overexpression increased HS production as demonstrated by HS ELISA (Fig. 5*B*) and immunocytochemistry (Fig. 5*C*). These data suggested that, in addition to syndecan-2 translocation, HS production is also involved in Epac-induced cell migration. To investigate the involvement of HS production in Epac-induced cell migration, we examined whether HS degradation inhibits cell migration. When the amount of HS was decreased enzymatically with heparitinase (Fig. 5*B*), both basal and Epac-induced cell migration were decreased (Fig. 5*D*). These data were further confirmed by decreased Epac-induced cell migration with sodium chlorate, which chemically degrades HS (data not shown).

We next explored the mechanism by which Epac increases HS production. We examined changes in expressions of HS-biosynthetic enzymes and found that Epac1 overexpression markedly increased expression of NDST-1 (Fig. 5*E*). We also found that Epac1 overexpression neither changes NDST-1 mRNA expression nor protein degradation (data not shown), but, rather, at the level of proteins, as shown by increased protein translation in [^{35}S]methionine pulse-labeling assay (Fig. 5*F*). We also examined whether deletion of NDST-1 decreases HS production and migration. When NDST-1 expression was reduced by siRNA (Fig. 5, *G* and *H*), both basal and Epac-induced HS production were decreased (Fig. 5*B*), paralleled with decreased basal- and Epac-induced cell migration (Fig. 5*D*). Put together, these data suggested that increased HS production with enhanced NDST-1 expression is involved in Epac-induced cell migration.

Epac increases melanoma metastasis to lung in mice. Migratory ability is essential for cancer metastasis not only in the detachment from cancer origin but also in transendothelial extravasation. To examine whether Epac-induced cell migration enhances melanoma metastasis, we performed lung colonization assay in mice, which can reflect the ability of extravasation (2, 46). In mouse Cloudman S91 melanoma cell line, Epac1 was endogenously expressed (Fig. 6*A*). Both 8-pMeOPT and Epac1 overexpression increased cell migration (Fig. 6*B*). We thus examined the effect of overexpression of Epac1 on melanoma metastasis. The number of metastatic colonies in the lung was significantly higher in the Epac1-overexpression group than in control group (GFP overexpression) (Fig. 6, *C* and *D*). These data suggested that Epac enhances melanoma metastasis presumably by increased cell migration.

DISCUSSION

The central finding of this study is that Epac increases melanoma cell migration/metastasis. The role of cAMP in melanoma metastasis is largely unknown. In the 1980s, a report demonstrated that intracellular cAMP positively correlates with the melanoma metastatic ability in mice (27). In contrast, treating melanoma cells with cholera toxin, which increases

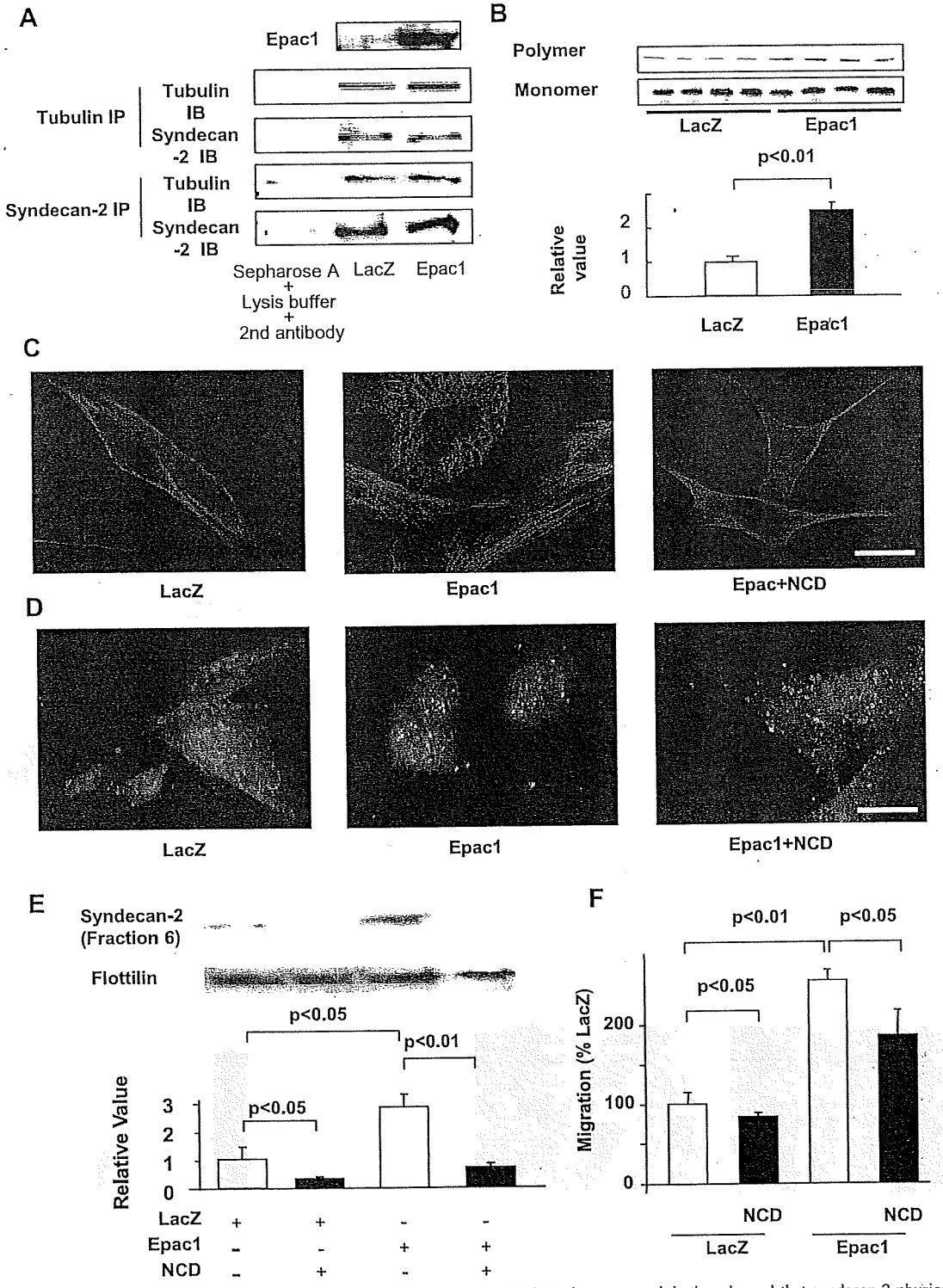

Fig. 3. Epac increases syndecan-2 translocation by tubulin polymerization in SK-Mel-2. *A*: immunoprecipitation showed that syndecan-2 physically interacts with tubulin; however, Epac1 overexpression did not enhance the binding between syndecan-2 and tubulin. Epac1 was increased by Epac1 overexpression (*top*). *B*: immunoblots showed that Epac1 overexpression increases polymer form of tubulin. A bar graph shows the densitometric analysis of ratios of tubulin polymers to tubulin monomers. $n = 4$. *C*: immunocytochemistry for tubulin (red) is shown. Epac1 overexpression increased fine tubulin network, and such network formation was inhibited by nocodazol (NCD, 10 μM). Scale bar, 3 μm. *D*: immunocytochemistry for syndecan-2 (red) and lipid rafts (green) is shown. NCD (10 μM) decreased Epac1-induced syndecan-2 colocalization with lipid rafts (yellow). Scale bar, 3 μm. *E*: immunoblot showed that NCD (10 μM) decreased basal and Epac overexpression-induced syndecan-2 expression in lipid rafts-rich fraction. $n = 4$. *F*: migration assay showed that NCD (10 μM) decreased basal and Epac1 overexpression-induced cell migration. $n = 4$.

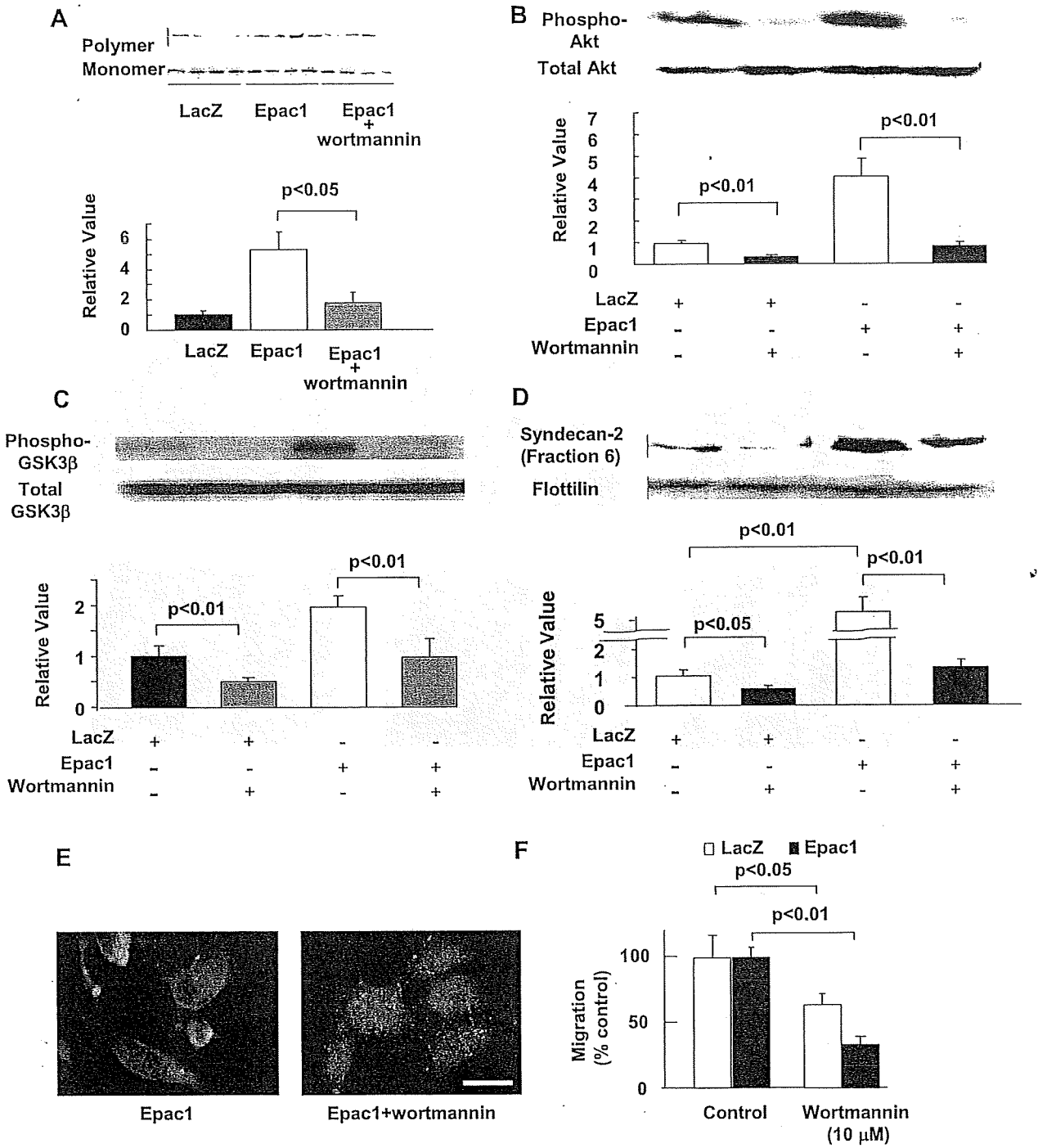

Fig. 4. Epac regulates tubulin polymerization via phosphoinositol-3 kinase (PI3K) in SK-Mel-2. *A–C*: immunoblots for polymer and monomer form of tubulin (*A*), phosphorylated and total form of Akt (*B*), or GSK3β (*C*) are shown. Bar graphs show densitometric analysis of ratios of tubulin polymers to tubulin monomers (*A*) and ratios of phosphorylated form and total protein (*B* and *C*). Wortmannin (10 μM) decreased Epac1-induced tubulin polymerization, basal and Epac1 overexpression-induced phosphorylation of Akt and GSK3β. $n = 4$. *D*: immunoblot showed that wortmannin (10 μM) decreased syndecan-2 expression in lipid rafts-rich fraction in cells with either LacZ or Epac1 overexpression. $n = 4$. *E*: immunocytochemistry for syndecan-2 (red) and lipid rafts (green) is shown. Wortmannin (10 μM) decreased Epac1 overexpression-induced syndecan-2 colocalization with lipid rafts (yellow). Scale bar, 3 μm. *F*: migration assay was performed in the presence or absence of wortmannin (10 μM). Wortmannin inhibited basal and Epac1-induced migration $n = 4$.

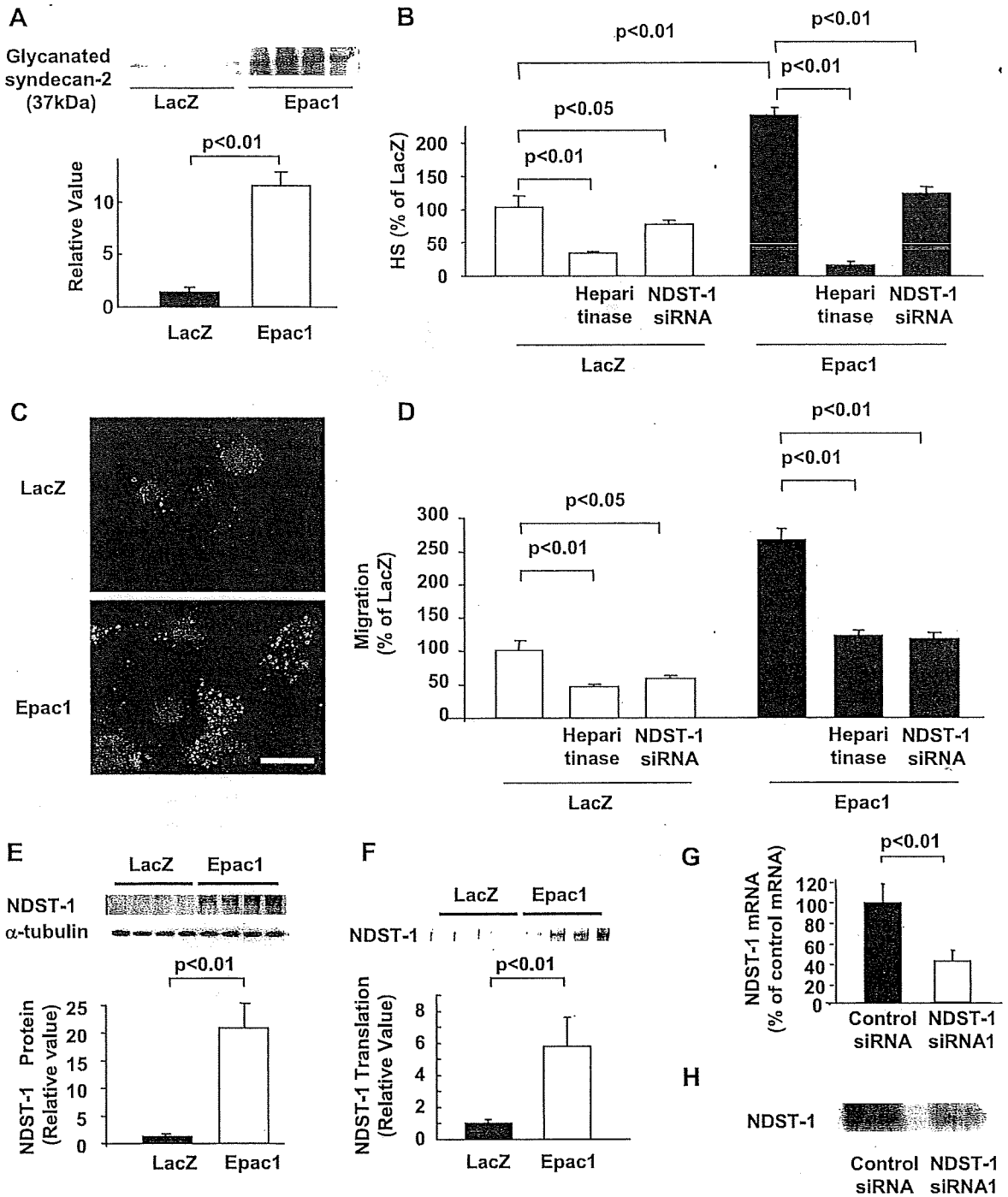

Fig. 5. Epac increases cell migration by heparin sulfate (HS) production in SK-Mel-2. *A*: immunoblot showed that Epac1 overexpression increased glycanated form of syndecan-2. $n = 4$. *B*: HS ELISA showed that amount of HS was increased by Epac1 overexpression. Both heparitinase (0.08 U/ml) and NDST-1 siRNA decreased basal and Epac1 overexpression-induced HS amount. $n = 4$. *C*: immunocytochemistry showed that HS (green) was increased in cells overexpressing Epac1. Scale bar, 3 μm. *D*: migration assay showed that both heparitinase (0.08 U/ml) and NDST1 siRNA decreased basal and Epac1 overexpression-induced cell migration. $n = 4$. *E*: immunoblot showed that NDST-1 expression was increased by Epac1 overexpression. $n = 4$. *F*: autoradiography of [^{35}S]methionine pulse labeling assay showed that NDST-1 protein translation was increased by Epac1 overexpression. $n = 4$. *G*: qPCR showed that NDST-1 siRNA decreased mRNA expression of NDST-1. $n = 4$. *H*: immunoblot showed that NDST-1 siRNA decreased protein expression of NDST-1.

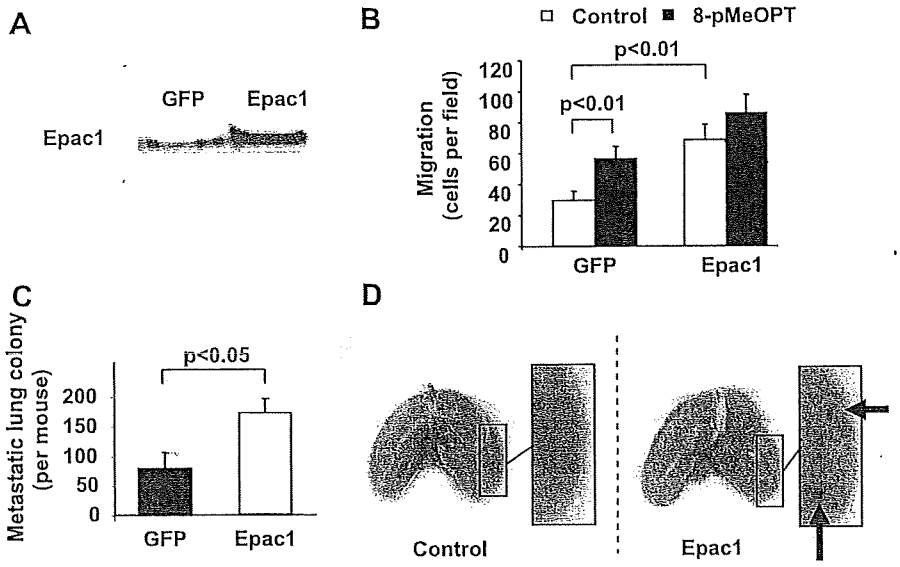

Fig. 6. Epac increases lung metastasis of Cloudman S91 melanoma in mice. *A*: immunoblot showed that Epac1 is endogenously expressed in S91 cells (*left lane*) and Epac1 adenovirus infection further increased Epac1 expression (*right lane*). *B*: migration assay showed that both 8-pMeOPT (50 μM) and Epac1 overexpression increased cell migration. $n = 4$. *C*: lung colonization assay demonstrated that the number of metastatic colonies was increased by Epac1 overexpression compared with control (GFP). $n = 10$. *D*: representative pictures of lungs from mice subjected to the melanoma cell injection are shown. Metastatic nodules on the lung surface are indicated by arrows.

cAMP, reduced melanoma colony formation in mice (33). To obtain data of the role of cAMP, we examined the effect of target proteins, i.e., PKA and Epac, on melanoma cell migration/metastasis. We demonstrated that Epac increases melanoma cell migration, but PKA did not. Epac also enhanced melanoma metastasis in mice, indicating that Epac plays a major role in enhancing the metastatic ability of melanoma cells.

We demonstrated that Epac regulates localization of syndecan-2. Syndecan is known to regulate cell migration in various cancer cells through its binding to extracellular HS (19). Syndecan-translocation to lipid rafts plays a role in cell migration (39). Lipid rafts are known to serve as platforms for molecules (42), and translocation of molecules, such as ICAM-1 (30), calpain (32), and integrins (25), to lipid rafts is necessary to activate cell migration. We demonstrated that Epac increased translocation of syndecan-2 to lipid rafts. Deletion of syndecan-2 as well as disruption of lipid rafts decreased Epac-induced cell migration. These data suggested that translocation of syndecan-2 to lipid rafts plays a major role in Epac-induced cell migration. We have also demonstrated that Epac increased glycanation of syndecan-2, which plays a role in connecting the cell surface to extracellular HS (19, 45). On the other hand, studies have demonstrated that the clustering of syndecan in lipid rafts/caveolae is necessary for enhancing cell migration (13). To examine involvement of syndecan-2 clustering in Epac-induced cell migration, further experiments, such as those using overexpression of recombinant syndecan-2 lacking PDZ domain, which mediates syndecan clustering (39), is required. In addition, recent reports have demonstrated that syndecans increases cell migration via integrin α2 (10), laminin α3 (1), focal adhesion formation, and protein kinase C (10). Further investigation may be required to examine whether Epac also regulates these syndecan-related mechanisms in cell migration.

It is also well known that microtubule formation plays a role in the transportation of molecules (15, 18). A previous report demonstrated that Epac increased tubulin growth by direct binding to tubulin (29). Our data, however, did not show interaction between Epac1 and tubulin in immunoprecipitation assays. Instead, we demonstrated that Epac increased tubulin polymerization via activation of the PI3K/Akt/GSK3β pathway. Since GSK3β plays a central role in tubulin polymerization (48, 49), it is reasonable to speculate that Epac mediates tubulin polymerization via the PI3K/Akt/GSK3β pathway.

Even though HS plays a central role in cell migration (14), little is known about the mechanism of HS production. We demonstrated that Epac stimulates HS production in melanoma cells by NDST-1 expression. Such Epac-induced NDST-1 expression occurs at the level of protein translation but not at the transcription level. As far as we know, this is the first report showing that a particular molecule, i.e., Epac, can enhance NDST-1 expression. On the other hand, a report showed that cAMP upregulates 3-*O*-sulfotransferase-1, a HS-biosynthesis enzyme, in F9 embryonic carcinoma cells (47); however, this is not the case in our study. We did not find that 3-*O*-sulfotransferase-1 was increased by Epac (data not shown). A remaining question is how Epac regulates NDST-1 translation. Since Epac stimulates GSK3β, which plays a major role in protein translation, it is tempting to speculate that Epac regulates NDST-1 translation via GSK3β. Indeed, our data showed that wortmannin decreased Epac-induced NDST-1 translation (data not shown), supporting the idea that Epac regulates protein translation via GSK3β.

Migratory ability increases as the melanoma stage progress; when migration was compared in human melanoma cell lines, migration was greater in metastatic melanoma than in primary melanoma (9). We showed that SK-Mel-24 cells, derived from metastatic lymph node melanoma, showed higher Epac1 expression than in SK-Mel-2 cells, derived from regional metastasis. Also, melanoma cell lines showed increased Epac1 expression than melanocytes. Accordingly, it is likely that Epac1 expression increases as melanoma stage progress and provides metastatic ability. However, we examined only two melanoma cell lines. Thus, to obtain conclusive evidence, further study, i.e., investigation of the relation between Epac expression and metastatic ability by the use of different stages of melanoma in

cell lines and/or human melanoma samples, is required to obtain conclusive evidence.

In conclusion, the robust finding of our study suggests that Epac may serve as a target molecule in melanoma cancer thereby inhibiting melanoma metastasis, even though we do not yet know whether Epac similarly regulates HS signaling in other cancer cell types.

ACKNOWLEDGMENTS

We thank Lauren Danridge for critical reading of the manuscript.

GRANTS

This study was supported in part by grants from the Japan Space Forum, the Japanese Ministry of Education, Culture, Sports, Science, and Technology, and the Takeda Science Foundation and National Institutes of Health Grants GM-067773 and HL-059139 (to Y. Ishikawa), and the American Heart Association (SDG 0835596D) and the Foundation of UMDNJ (K. Iwatsubo).

REFERENCES

1. **Araki E, Momota Y, Togo T, Tanioka M, Hozumi K, Nomizu M, Miyachi Y, Utani A.** Clustering of Syndecan-4 and integrin β1 by laminin α3 chain-derived peptide promotes keratinocyte migration. *Mol Biol Cell* 20: 3012–3024, 2009.
2. **Bellahcene A, Castronovo V, Ogbureke KU, Fisher LW, Fedarko NS.** Small integrin-binding ligand N-linked glycoproteins (SIBLINGs): multifunctional proteins in cancer. *Nat Rev Cancer* 8: 212–226, 2008.
3. **Benoist F and Grand-Perret T.** Cotranslational degradation of apolipoprotein B100 by the proteasome is prevented by microsomal triglyceride transfer protein synchronized translation studies on HepG2 cells treated with an inhibitor of microsomal triglyceride transfer protein. *J Biol Chem* 272: 20435–20442, 1997.
4. **Bernfield M, Gotte M, Park PW, Reizes O, Fitzgerald ML, Lincecum J, Zako M.** Functions of cell surface heparan sulfate proteoglycans. *Ann Rev Biochem* 68: 729–777, 1999.
5. **Berwick M, Wiggins C.** The current epidemiology of cutaneous malignant melanoma. *Front Biosci* 11: 1244–1254, 2006.
6. **Bos JL.** Epac proteins: multi-purpose cAMP targets. *Trends Biochem Sci* 31: 680–686, 2006.
7. **Brennesvik EO, Ktori C, Ruzzin J, Jebens E, Shepherd PR, Jensen J.** Adrenaline potentiates insulin-stimulated PKB activation via cAMP and Epac: implications for cross talk between insulin and adrenaline. *Cell Signal* 17: 1551–1559, 2005.
8. **Brockstedt U, Dobra K, Nurminen M, Hjerpe A.** Immunoreactivity to cell surface syndecans in cytoplasm and nucleus: tubulin-dependent rearrangements. *Exp Cell Res* 274: 235–245, 2002.
9. **Byers HR, Etoh T, Doherty JR, Sober AJ, Mihm MC Jr.** Cell migration and actin organization in cultured human primary, recurrent cutaneous and metastatic melanoma. Time-lapse and image analysis. *Am J Pathol* 139: 423–435, 1991.
10. **Choi S, Kim Y, Park H, Han IO, Chung E, Lee SY, Kim YB, Lee JW, Oh ES, Yi JY.** Syndecan-2 overexpression regulates adhesion and migration through cooperation with integrin alpha2. *Biochem Biophys Res Commun* 384: 231–235, 2009.
11. **Claffey KP, Brown LF, del Aguila LF, Tognazzi K, Yeo KT, Manseau EJ, Dvorak HF.** Expression of vascular permeability factor/vascular endothelial growth factor by melanoma cells increases tumor growth, angiogenesis, and experimental metastasis. *Cancer Res* 56: 172–181, 1996.
12. **de Rooij J, Zwartkruis FJ, Verheijen MH, Cool RH, Nijman SM, Wittinghofer A, Bos JL.** Epac is a Rap1 guanine-nucleotide-exchange factor directly activated by cyclic AMP. *Nature* 396: 474–477, 1998.
13. **Ethell IM, Yamaguchi Y.** Cell surface heparan sulfate proteoglycan syndecan-2 induces the maturation of dendritic spines in rat hippocampal neurons. *J Cell Biol* 144: 575–586, 1999.
14. **Fjeldstad K, Kolset SO.** Decreasing the metastatic potential in cancers–targeting the heparan sulfate proteoglycans. *Curr Drug Targets* 6: 665–682, 2005.
15. **Galbraith JA, Gallant PE.** Axonal transport of tubulin and actin. *J Neurocytol* 29: 889–911, 2000.
16. **Gao L, Feng Y, Bowers R, Becker-Hapak M, Gardner J, Council L, Linette G, Zhao H, Cornelius LA.** Ras-associated protein-1 regulates extracellular signal-regulated kinase activation and migration in melanoma cells: two processes important to melanoma tumorigenesis and metastasis. *Cancer Res* 66: 7880–7888, 2006.
17. **Hadjidemetriou S, Toomre D, Duncan J.** Motion tracking of the outer tips of microtubules. *Med Image Anal* 2008.
18. **Head BP, Patel HH, Roth DM, Murray F, Swaney JS, Niesman IR, Farquhar MG, Insel PA.** Microtubules and actin microfilaments regulate lipid raft/caveolae localization of adenylyl cyclase signaling components. *J Biol Chem* 281: 26391–26399, 2006.
19. **Iozzo RV.** Series Introduction: Heparan sulfate proteoglycans: intricate molecules with intriguing functions. *J Clin Invest* 108: 165–167, 2001.
20. **Iwatsubo K, Minamisawa S, Tsunematsu T, Nakagome M, Toya Y, Tomlinson JE, Umemura S, Scarborough RM, Levy DE, Ishikawa Y.** Direct inhibition of type 5 adenylyl cyclase prevents myocardial apoptosis without functional deterioration. *J Biol Chem* 279: 40938–40945, 2004.
21. **Iwatsubo K, Suzuki S, Li C, Tsunematsu T, Nakamura F, Okumura S, Sato M, Minamisawa S, Toya Y, Umemura S, Ishikawa Y.** Dopamine induces apoptosis in young, but not in neonatal, neurons via Ca^{2+}-dependent signal. *Am J Physiol Cell Physiol* 293: C1498–C1508, 2007.
22. **Jing H, Yen JH, Ganea D.** A novel signaling pathway mediates the inhibition of CCL3/4 expression by prostaglandin E2. *J Biol Chem* 279: 55176–55186, 2004.
23. **Kawabe J, Okumura S, Lee MC, Sadoshima J, Ishikawa Y.** Translocation of caveolin regulates stretch-induced ERK activity in vascular smooth muscle cells. *Am J Physiol Heart Circ Physiol* 286: H1845–H1852, 2004.
24. **Kopatz I, Remy JS, Behr JP.** A model for non-viral gene delivery: through syndecan adhesion molecules and powered by actin. *J Gene Med* 6: 769–776, 2004.
25. **Krauss K, Altevogt P.** Integrin leukocyte function-associated antigen-1-mediated cell binding can be activated by clustering of membrane rafts. *J Biol Chem* 274: 36921–36927, 1999.
26. **Leitinger B, Hogg N.** The involvement of lipid rafts in the regulation of integrin function. *J Cell Sci* 115: 963–972, 2002.
27. **Lester BR, Greig RG, Buscarino C, Sheppard JR, Corwin SP, Poste G.** cAMP metabolism in B16 melanoma clones during the formation of experimental and spontaneous metastases. *Int J Cancer* 38: 405–411, 1986.
28. **Lorenowicz MJ, van Gils J, de Boer M, Hordijk PL, and Fernandez-Borja M.** Epac1-Rap1 signaling regulates monocyte adhesion and chemotaxis. *J Leukoc Biol* 80: 1542–1552, 2006.
29. **Mei FC, Cheng X.** Interplay between exchange protein directly activated by cAMP (Epac) and microtubule cytoskeleton. *Mol BioSys* 1: 325–331, 2005.
30. **Millan J, Hewlett L, Glyn M, Toomre D, Clark P, Ridley AJ.** Lymphocyte transcellular migration occurs through recruitment of endothelial ICAM-1 to caveola- and F-actin-rich domains. *Nat Cell Biol* 8: 113–123, 2006.
31. **Misra UK, Pizzo SV.** Coordinate regulation of forskolin-induced cellular proliferation in macrophages by protein kinase A/cAMP-response element-binding protein (CREB) and Epac1-Rap1 signaling: effects of silencing CREB gene expression on Akt activation. *J Biol Chem* 280: 38276–38289, 2005.
32. **Nuzzi PA, Senetar MA, Huttenlocher A.** Asymmetric localization of calpain 2 during neutrophil chemotaxis. *Mol Biol Cell* 18: 795–805, 2007.
33. **Ormerod EJ, Hart IR.** Different growth responses to agents which elevate cAMP in human melanoma cell lines of high and low experimental metastatic capacity. *Clin Exp Metast* 7: 85–95, 1989.
34. **Oshikawa J, Otsu K, Toya Y, Tsunematsu T, Hankins R, Kawabe J, Minamisawa S, Umemura S, Hagiwara Y, Ishikawa Y.** Insulin resistance in skeletal muscles of caveolin-3-null mice. *Proc Natl Acad Sci USA* 101: 12670–12675, 2004.
35. **Qiao D, Meyer K, Mundhenke C, Drew SA, Friedl A.** Heparan sulfate proteoglycans as regulators of fibroblast growth factor-2 signaling in brain endothelial cells. Specific role for glypican-1 in glioma angiogenesis. *J Biol Chem* 278: 16045–16053, 2003.
36. **Raats CJI, Bakker MAH, van den Born J, Berden JHM.** Hydroxyl radicals depolymerize glomerular heparan sulfate in vitro and in experimental nephrotic syndrome. *J Biol Chem* 272: 26734–26741, 1997.
37. **Rickard A, Portell C, Siegal J, Goeckeler Z, Lagunoff D.** Measurement of the motility of endothelial cells in confluent monolayers. *Microcirculation* 10: 193–203, 2003.
38. **Thomas LA, Yamada KM.** Contact stimulation of cell migration. *J Cell Sci* 103: 1211–1214, 1992.

39. **Tkachenko E, Elfenbein A, Tirziu D, Simons M.** Syndecan-4 clustering induces cell migration in a PDZ-dependent manner. *Circ Res* 98: 1398–1404, 2006.
40. **Tkachenko E, Simons M.** Clustering induces redistribution of syndecan-4 core protein into raft membrane domains. *J Biol Chem* 277: 19946–19951, 2002.
41. **Ulucan C, Wang X, Baljinnyam E, Bai Y, Okumura S, Sato M, Minamisawa S, Hirotani S, Ishikawa Y.** Developmental changes in gene expression of Epac and its upregulation in myocardial hypertrophy. *Am J Physiol Heart Circ Physiol* 293: H1662–H1672, 2007.
42. **Williams TM, Lisanti MP.** The Caveolin genes: from cell biology to medicine. *Ann Med* 36: 584–595, 2004.
43. **Wolter KG, Verhaegen M, Fernandez Y, Nikolovska-Coleska Z, Riblett M, de la Vega CM, Wang S, Soengas MS.** Therapeutic window for melanoma treatment provided by selective effects of the proteasome on Bcl-2 proteins. *Cell Death Differ* 14: 1605–1616, 2007.
44. **Yokoyama U, Minamisawa S, Quan H, Ghatak S, Akaike T, Segi-Nishida E, Iwasaki S, Iwamoto M, Misra S, Tamura K, Hori H, Yokota S, Toole BP, Sugimoto Y, Ishikawa Y.** Chronic activation of the prostaglandin receptor EP4 promotes hyaluronan-mediated neointimal formation in the ductus arteriosus. *J Clin Invest* 116: 3026–3034, 2006.
45. **Yoneda A, Couchman JR.** Regulation of cytoskeletal organization by syndecan transmembrane proteoglycans. *Matrix Biol* 22: 25–33, 2003.
46. **Yu HR, Schultz RM.** Relationship between secreted urokinase plasminogen activator activity and metastatic potential in murine B16 cells transfected with human urokinase sense and antisense genes. *Cancer Res* 50: 7623–7633, 1990.
47. **Zhang L, Schwartz JJ, Miller J, Liu J, Fritze LMS, Shworak NW, Rosenberg RD.** The retinoic acid and cAMP-dependent up-regulation of 3-*O*-sulfotransferase-1 leads to a dramatic augmentation of anticoagulantly active heparan sulfate biosynthesis in F9 embryonal carcinoma Cells. *J Biol Chem* 273: 27998–28003, 1998.
48. **Zhou FQ, Snider Cell biology WD.** GSK-3beta and microtubule assembly in axons. *Science* 308: 211–214, 2005.
49. **Zumbrunn J, Kinoshita K, Hyman AA, Nathke IS.** Binding of the adenomatous polyposis coli protein to microtubules increases microtubule stability and is regulated by GSK3 beta phosphorylation. *Curr Biol* 11: 44–49, 2001.

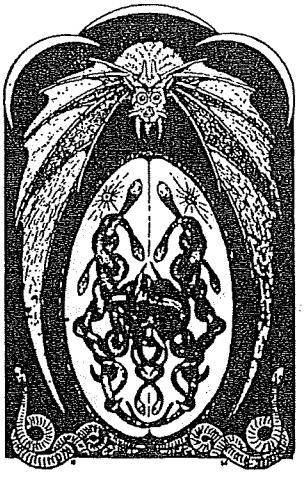

THE JOURNAL OF BIOLOGICAL CHEMISTRY VOL. 284, NO. 45, pp. 31431–31440, November 6, 2009

Activator of G Protein Signaling 8 (AGS8) Is Required for Hypoxia-induced Apoptosis of Cardiomyocytes

ROLE OF Gβγ AND CONNEXIN 43 (CX43)[*][S]

Received for publication, April 30, 2009, and in revised form, August 13, 2009 Published, JBC Papers in Press, September 1, 2009, DOI 10.1074/jbc.M109.014068

Motohiko Sato[‡1,2], Qibin Jiao[‡1], Takashi Honda[‡], Reiko Kurotani[‡], Eiji Toyota[§], Satoshi Okumura[‡], Tatsuo Takeya[¶], Susumu Minamisawa[‖], Stephen M. Lanier[**], and Yoshihiro Ishikawa[‡3]

From the [‡]Cardiovascular Research Institute, Yokohama City University School of Medicine, Fukuura, Yokohama 236-0004, Japan, the [§]Department of of Cardiology, Kawasaki Medical School, Kurashiki 701-0192, Japan, the [¶]Graduate School of Biological Sciences, Nara Institute of Science and Technology, Nara 630-0101, Japan, the [‖]Department of Life Science and Medical Bioscience, Waseda University, Tokyo 162-8480, Japan, and the [**]Department of Pharmacology, Medical University of South Carolina, Charleston, South Carolina 29425

Ischemic injury of the heart is associated with activation of multiple signal transduction systems including the heterotrimeric G-protein system. Here, we report a role of the ischemia-inducible regulator of Gβγ subunit, AGS8, in survival of cardiomyocytes under hypoxia. Cultured rat neonatal cardiomyocytes (NCM) were exposed to hypoxia or hypoxia/reoxygenation following transfection of AGS8siRNA or pcDNA::AGS8. Hypoxia-induced apoptosis of NCM was completely blocked by AGS8siRNA, whereas overexpression of AGS8 increased apoptosis. AGS8 formed complexes with G-proteins and channel protein connexin 43 (CX43), which regulates the permeability of small molecules under hypoxic stress. AGS8 initiated CX43 phosphorylation in a Gβγ-dependent manner by providing a scaffold composed of Gβγ and CX43. AGS8siRNA blocked internalization of CX43 following exposure of NCM to repetitive hypoxia; however it did not influence epidermal growth factor-mediated internalization of CX43. The decreased dye flux through CX43 that occurred with hypoxic stress was also prevented by AGS8siRNA. Interestingly, the Gβγ inhibitor Gallein mimicked the effect of AGS8 knockdown on both the CX43 internalization and the changes in cell permeability elicited by hypoxic stress. These data indicate that AGS8 is required for hypoxia-induced apoptosis of NCM, and that AGS8-Gβγ signal input increased the sensitivity of cells to hypoxic stress by influencing CX43 regulation and associated cell permeability. Under hypoxic stress, this unrecognized response program plays a critical role in the fate of NCM.

G-protein-coupled receptors (GPCRs)[4] are signaling proteins on the cell surface responsible for mediating various ligands, such as hormones and neurotransmitters. Activation of cell surface GPCRs initiates nucleotide exchange on Gα subunits, which leads to a conformational change of Gαβγ and subsequent transduction of signals to various intracellular effector molecules (1–3). In addition to such established signaling pathways, recent studies indicate the existence of a novel class of regulatory proteins for heterotrimeric G-proteins. These regulatory proteins may provide alternative signal processing via Gαβγ, Gα, or Gβγ subunits distinct from typical GPCR pathways, and identifying these mechanisms may uncover unrecognized roles of G-proteins beyond simple transducers of signals from GPCRs (4–6).

During the alteration of signaling pathways in disease states, such regulatory proteins may be involved in adaptation programs of cells to maintain homeostasis (7–11). Genetic modification of regulatory proteins for G-proteins leads to the development of cardiovascular dysfunction in mice including hypertension, maladaptive response to pressure overload, or altered baroreceptor reflex (9, 12, 13). Thus, such regulatory accessory proteins may be involved in the development of disease via either regulating GPCR-initiated signals or by undefined, alternative G-protein signaling pathways operating independent of the receptor.

In our efforts to adaptation-specific signal regulators for G-protein systems, we identified a novel receptor-independent G-protein activator, activator of G-protein signaling 8 (AGS8), from a cDNA library of rat hearts subjected to repetitive transient ischemia with the development of collateral vessels (8). Initial observations indicated that AGS8 was up-regulated in cardiomyocytes in response to transient ischemia and hypoxia.

* This work was supported, in whole or in part, by National Institutes of Health Grants NS24821 and DA025896 (to S. M. L.). This work was also supported by Grants-in-Aid for Scientific Research (C) 18599006 and 20590212 (to M. S.) and 18057018 and 193902217 (to Y. I.), the Yokohama Foundation for Advancement of Medical Science (to M. S.), grants from the Strategic Research Project K18017 and K19021 of Yokohama City University, Japan (to M. S.), and a grant from the Takeda Science Foundation (to Y. I.).

[S] The on-line version of this article (available at http://www.jbc.org) contains supplemental materials and Figs. S1 and S2.

[1] Both authors contributed equally to the studies presented in this report.

[2] Recipient of grants from the Takeda Science Foundation, NOVARTIS Foundation (Japan) for the Promotion of Science, Mitsubishi Pharma Research Foundation, The Ichiro Kanehara Foundation, and Mochida Memorial Foundation for Medical and Pharmaceutical Research. To whom correspondence may be addressed: Cardiovascular Research Institute, Yokohama City University School of Medicine, 3-9 Fukuura, Kanazawa-Ku, Yokohama 236-0004, Japan. Fax: 1-81-45-788-1470; E-mail: motosato@yokohama-cu.ac.jp.

[3] To whom correspondence may be addressed: Fax: 1-81-45-788-1470; E-mail: yishikaw@med.yokohama-cu.ac.jp.

[4] The abbreviations used are: GPCR, G-protein-coupled receptor; AGS8, activator of G protein signaling 8; CX43, connexin 43; NCM, neonatal cardiomyocyte; siRNA, small interfering RNA; LY, lucifer yellow; EGF, epidermal growth factor; GST, glutathione *S*-transferase; TUNEL, terminal deoxynucleotidyltransferase-mediated dUTP nick end-labeling; DAPI, 4′,6-diamidino-2-phenylindole; analysis of variance.